Energy & Environmental Science

REVIEW

View Article Online
View Journal | View Issue

Cite this: *Energy Environ. Sci.*, 2017, **10**, 2284

Impact of H_2O on organic–inorganic hybrid perovskite solar cells

Jianbing Huang, *[a] Shunquan Tan, [bc] Peter D. Lund [d] and Huanping Zhou [c]

The performance and stability of organic–inorganic hybrid perovskite solar cells (PSCs) is sensitive to water and moisture in an ambient environment. Understanding how H_2O influences the perovskite material is also important for developing appropriate control strategies to mitigate the problem. Here we provide a comprehensive review on the effect of water on the state-of-the-art lead-based perovskite solar cells in terms of perovskite material design, perovskite film preparation, device fabrication, and photovoltaic application. It is found that a moderate amount of water can facilitate nucleation and crystallization of the perovskite material, resulting in better perovskite film quality and enhanced PSC performance. The perovskite materials are irreversibly destroyed by H_2O after a certain level of water, but they exihibit better tolerance than initially expected. Humidity resistant fabrication of high-performance PSC devices and modules should therefore be favoured. Generally, water shows a negative effect on the long-term stability and lifetime of PSCs. To reduce the effects from water during outdoor operation, attention should be paid to different protection methods such as varying the perovskite composition, optimizing the electron/hole transport layer and encapsulation of the device.

Received 15th June 2017,
Accepted 21st September 2017

DOI: 10.1039/c7ee01674c

rsc.li/ees

[a] *State Key Laboratory of Multiphase Flow in Power Engineering, School of Energy and Power Engineering, Xi'an Jiaotong University, P. R. China. E-mail: huangjb@mail.xjtu.edu.cn; Fax: +86-29-82669033; Tel: +86-29-82665591*
[b] *School of Chemical Engineering and Technology, Xi'an Jiaotong University, P. R. China*
[c] *Department of Materials Science and Engineering, College of Engineering, Peking University, P. R. China*
[d] *Department of Engineering Physics/Advanced Energy Systems, School of Science, Aalto University, Espoo, FI-00076 AALTO, Finland*

1. Introduction

In 2009 an organic–inorganic hybrid perovskite material was incorporated into a dye-sensitized solar cell (DSSC) as a light absorber for the first time. Though the initial efficiency was low (3.8%), the new material exhibited good crystallinity, suitable optical properties, and unique electronic properties.[1] By optimizing the fabrication process, choosing new core materials, and designing a better photovoltaic device structure, the energy

Jianbing Huang

Jianbing Huang received his PhD degree in Chemical Engineering and Technology in 2008 from Tsinghua University, China. He is currently an Associate Professor at the State Key Laboratory of Multiphase Flow in Power Engineering, School of Energy and Power Engineering, Xi'an Jiaotong University, China. His research interests include solid state ionics, new energy materials, thermochemical hydrogen production, and combined heat and power from renewable energy.

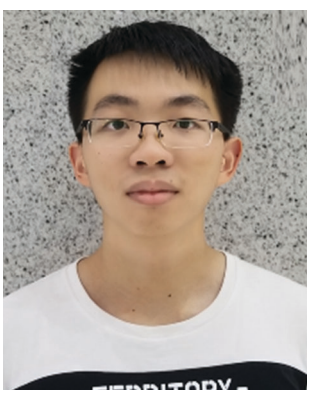

Shunquan Tan

Shunquan Tan received his BS degree in September 2017, majoring in Chemical Engineering at Xi'an Jiaotong University. He currently works as a research associate in Peking University. His research interests mainly focus on renewable energy and relevant materials, including perovskite materials and perovskite solar cells.

conversion efficiency of perovskite solar cells (PSCs) has recently achieved a value of >22%.[2]

The light-harvesting perovskite material $RAMX_3$ commonly refers to a 3D organic–inorganic hybrid compound in which RA is a monovalent organic cation (methylammonium ($CH_3NH_3^+$, MA^+), or formamidinium ($HN=CHNH_3^+$, FA^+)), M is a bivalent metal (Pb^{2+}, Sn^{2+}), and X is mostly a halide anion (Cl^-, Br^- or I^-). Capable of being mixed with cations (*e.g.* adding FA^+ into $MAPbI_3$ or partially replacing Pb^{2+} with Sn^{2+}) or anions (*e.g.* mixing various halides) in crystal units, $RAMX_3$ can be adjusted to obtain a moderate bandgap (E_g) for a single junction solar cell (1.1–1.4 eV) or tandem solar cell (~1.8 eV).[3] For example, $MAPbI_3$ possesses the lowest E_g of 1.6 eV.[4] A suitable bandgap could cover most of the visible light region from ~400 nm to 800 nm, and potentially expand to the infrared region.[5] In addition, the diffusion length, carrier lifetime, and mobility, though these vary by composition, are apt for separation and collection of charge carriers in solar cell devices.

$RAMX_3$ perovskites possess intrinsically simple growth kinetics, and PSCs resemble other thin film solar cells in terms of their device structures and materials to some extent, which make PSCs easy to be fabricated and potentially a low-cost photovoltaic technology.[6,7] The device architecture of PSCs can be divided into two distinct types: regular n–i–p PSCs and inverted p–i–n PSCs. In this review, unlike in most of the previous studies, we consider an integrated architecture shown in Fig. 1: electrode/second functional layer (SFL)/perovskite/first functional layer (FFL)/transparent conductive oxide (TCO) substrate. Here, FFL refers to the functional layer between the perovskite and TCO substrate, and SFL refers to the functional layer between the perovskite and electrode. In the n–i–p architecture, the FFL can accept and transport photoexcited electrons, generally using metal oxides such as ZnO, TiO_2 (mesoporous and planar) *etc.* Correspondingly, the SFL acts as a hole selective acceptor. Inversely, in the p–i–n architecture the FFL is used to separate the excited holes and deliver them toward the TCO and the SFL is responsible for the transport of electrons.

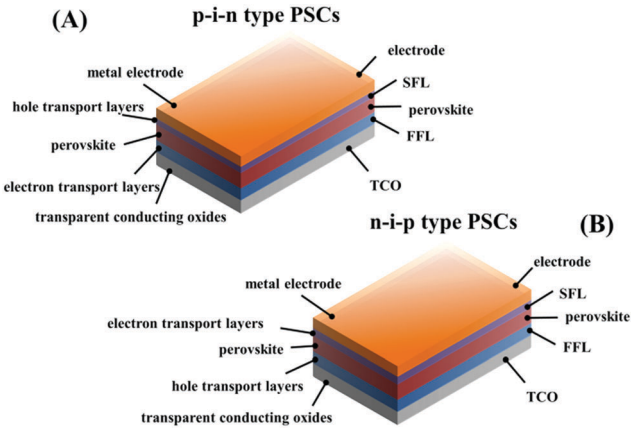

Fig. 1 Schematic of different PSC device architectures.

Though the efficiency of PSCs is comparable to that of commercial solar cells (*e.g.* mc-Si, c-Si, CdTe),[8,9] one of the major barriers in front of their commercialization is the poor material and device stability.[10–12] A great deal of studies show that the PSC is very likely to degrade in an ambient environment. Moisture (or water) is one of the major degradation triggers for the perovskite material itself and the PSC.

In earlier studies, H_2O was widely regarded as harmful to $MAPbI_3$ perovskite by turning it back to PbI_2 and MAI irreversibly, which results in loss of optical absorption and severe electron–hole recombination. However, Zhou *et al.* in 2014 reported that annealing under humid conditions could actually greatly improve the film quality and its electronic behavior, demonstrating a positive role of water.[13] Later, many studies have proposed that H_2O may have both advantageous and disadvantageous effects

Peter D. Lund

Dr Peter D. Lund is a Professor in Advanced Energy Systems at Aalto University, Finland. He has close to 40 years of experience in energy technologies, including solar and fuel cells. He has had visiting positions in China and Germany. Dr Lund is active in senior roles within European Union energy initiatives: he has chaired the Advisory Group Energy of European Commission and chairs the Energy Steering Panel of European Academies Science Advisory Council. He has served in an advisory role for many energy programs worldwide. He is member of the Swedish Engineering Academy in Finland. Dr Lund is the editor of several journals. He has given many invited talks, published 500 research papers, and received several awards, the latest being the Jinling Award in 2016.

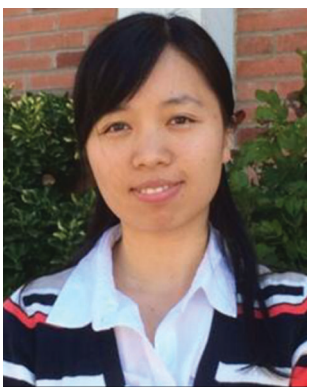

Huanping Zhou

Prof. Huanping Zhou received her PhD degree in inorganic chemistry from Peking University in 2010. After that, she joined the University of California, Los Angeles, as a postdoctoral researcher from 2010 to 2015. From July 2015, she joined Peking University as an assistant professor in the Department of Materials Science and Engineering, College of Engineering via "Young Thousand Talent Program". She is a materials chemist with expertise in the fields of nanoscience, thin film optoelectronics, organic/inorganic interface engineering, and the development and fabrication of related devices, such as photovoltaic cells, TFTs, etc. Currently, her research lab is focused on thin film optoelectronics, e.g., perovskite materials and solar cells.

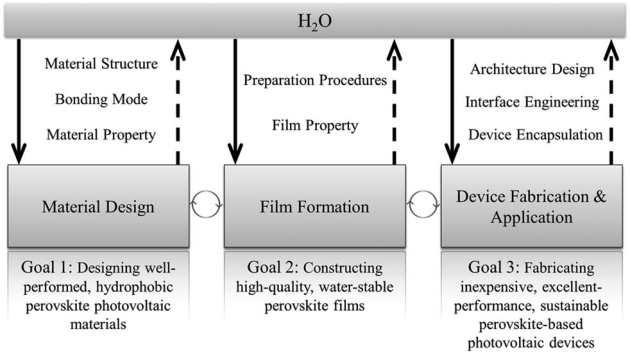

Fig. 2 Structure of the review. Highlighting the role of water in perovskite materials from different aspects.

on $RAMX_3$ perovskites and PSCs. However, comprehensive understanding of the role of H_2O in organic–inorganic hybrid perovskites and PSCs has seldom been discussed in previous reviews. Here we review the effect of water on the state-of-the-art lead-based perovskite solar cells from a broad perspective, covering perovskite material design, perovskite film preparation, device fabrication, and application to pave the way for the development of high-performance and reliable PSCs. The structure of the review is illustrated in Fig. 2.

This review discusses the impact of water on lead-based perovskite solar cells in perovskite material preparation and operation stages, but also relevant strategies for improving their resistance against water. The preparation routes for the formation of perovskite films are considered with a discussion on how water in various states affects crystallization and film quality. Water-induced degradation routes will be comprehensively reviewed along with the final chemical products, and optical and electronic properties. Furthermore, based on the water-induced degradation mechanisms, several approaches will be provided for better moisture resistance.

2. H_2O in perovskite film preparation

Preparation of a perovskite film requires multiple steps: formation and collection of perovskite ingredients, preparation of perovskite precursors, and perovskite film growth, all of which provide opportunities for intrusion of H_2O. Therefore, for a better understanding of possible routes for water penetration, we first describe the representative deposition methods with the related crystallization mechanisms.

2.1 Film preparation methods

A smooth, pinhole-free and highly crystalline $RAMX_3$ perovskite film is generally prepared by four representative processes (see Fig. 3A using $MAPbI_3$ as an example): one-step solution deposition (OSSD), sequential solution deposition (SSD), dual-source vapour deposition (DSVD), and vapour-assisted solution deposition (VASD).[1,7,14–17]

2.1.1 One-step solution deposition (OSSD). OSSD is implemented with the first step that RAX (RA = methylammonium, formamidinium) and PbX_2 (X = I, Br, Cl) simultaneously at the mole ratio of 1 : 1 or 3 : 1 are added to polar solvents (DMF, DMSO, GBL, *etc.*).[1,18] After stirring constantly at a certain temperature, the clear solution is spin coated or drop coated on the first functional layer. This is followed by annealing the as-formed perovskite film to evaporate solvents and ensure the crystallization of $RAPbX_3$.

Perovskite films in OSSD experience different crystallization growth mechanisms depending on the annealing temperature and annealing time.[19,20] When the substrate temperature is at or below 100 °C, the perovskite film experiences a multistage formation mechanism with three stages: the initial solution stage, the transition-to-solid film stage, and the transformation stage from intermediates into a crystalline perovskite film; however, when the substrate temperature is increased from 100 to 180 °C, the formation mechanism of the perovskite film is changed to the "direct formation mechanism".[19] An approximate time scale for each one of the stages and their evolution was established during the annealing of $MAPbI_3$ films at 100 °C in air, including the nucleation of small crystallites (i), a transitional stage during which a large number of grain boundaries are formed as precursors vanish (ii), an actual crystal growth period where different crystals coalesce (iii), and a final stage (iv) where the material is eventually formed.[20] In addition, a hot-casting technique at 180 °C was developed, during which the high substrate temperature at spin coating induces the formation of perovskite crystals. It was recently proposed that a Volmer–Weber growth mechanism occurs with island shaped grains, followed by integration into perovskite films.[21]

2.1.2 Sequential solution deposition (SSD). SSD is a two-step deposition method in which RAX and PbX_2 are dissolved in solvents separately.[14] The PbI_2 DMF solution is spin-coated and forms a PbI_2 film at first, then transforms into a $MAPbI_3$ film by reacting with the MAI iso-propanol solution. Annealing is normally needed to completely transform the unreacted PbI_2 to $MAPbI_3$.

Fu *et al.* reported two crystallization formation routes for SSD, depending on the concentration of MAI in iso-propanol (Fig. 4).[22] When the concentration of MAI is lower than 8 mg mL^{-1}, a solid–liquid interfacial mechanism takes place and the as-formed $MAPbI_3$ film will gradually block the MA^+ from further reacting with the inner PbI_2; whereas, a dissolution–recrystallization pathway occurs at >10 mg mL^{-1} MAI solution, during which a quick formed $MAPbI_3$ film covers the PbI_2 surface immediately, demanding longer reaction time or higher MAI concentration to fulfill the reaction *via* the formation of Pb_4^{2-}. It should be also noted that similar competing pathways are proposed to control the growth of freestanding $MAPbI_3$ crystals, *in situ* transformation and dissolution–crystallization mechanisms.[23]

2.1.3 Dual-source vapour deposition (DSVD). Vapor-based deposition techniques in which the ingredients are converted to gaseous states, reproducibly produce high-quality and dense perovskite films. DSVD, a dual chemical vapor source deposition technique, was developed by Snaith and his colleagues in which MAI and $PbCl_2$ precursor salts are co-evaporated under vacuum to deposit a $MAPbI_{3-x}Cl_x$ film followed by further annealing to realize full crystallization.[15] Afterwards, a sequential evaporation

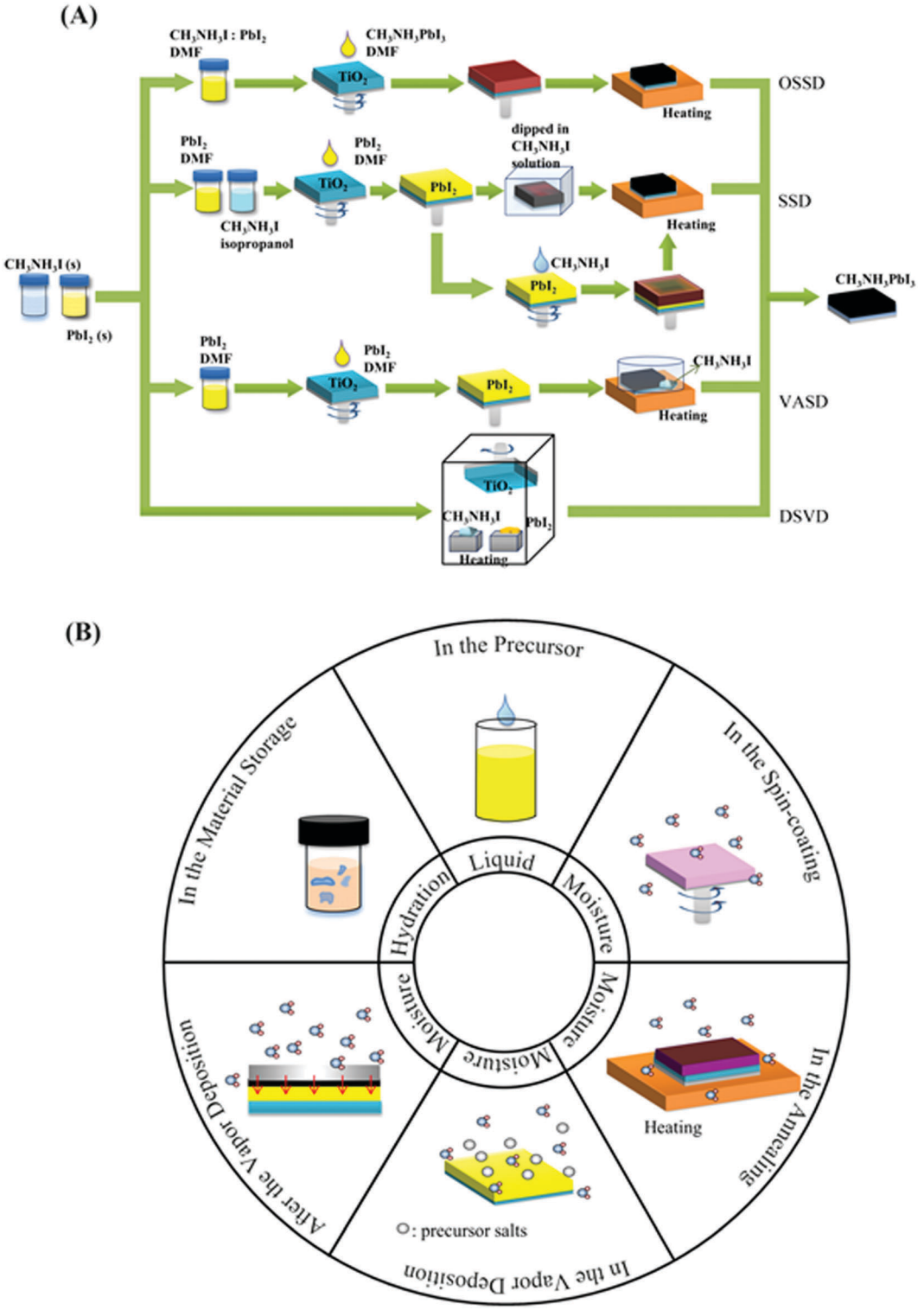

Fig. 3 (A) Preparation methods of perovskite films. (B) Comprehensive overview of the existence of water molecules in the preparation steps.

method and chemical vapor deposition were developed as DSVD derivatives.[24,25] With a higher Cl content ($y \sim 0.5$), the $MAPb(I_{1-y}Cl_y)_3$ phase become transparent and greenish. At low Cl content ($y < 0.05$), $MAPb(I_{1-y}Cl_y)_3$ shows dark perovskite phases. This indicates that the miscibility gap for $MAPbI_3$–$MAPbCl_3$ mixtures is in the range of $0.05 < y < 0.5$.[26] The dark $MAPb(I_{1-y}Cl_y)_3$ ($y = \sim 0.02$) perovskite exhibits 3-dimensional growth in the initial stage, and then it maintains a cubic phase, while $MAPbI_3$ at first also experiences 3D growth, but gradually shows a domain tetragonal structure.[27]

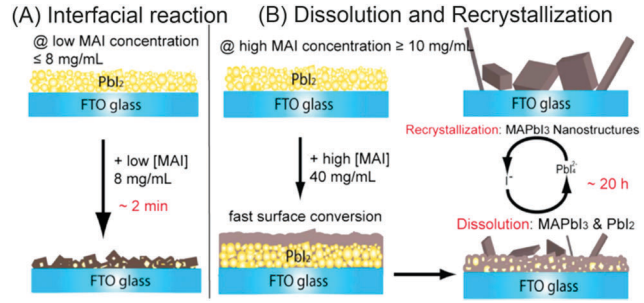

Fig. 4 (A) Interfacial reaction mechanism at lower MAI concentrations. (B) Dissolution–recrystallization growth mechanism at higher MAI concentrations. The conversion *via* interfacial reaction is faster than dissolution–recrystallization growth. Adapted from ref. 22, Copyright 2015 American Chemical Society.

2.1.4 Vapour-assisted solution deposition (VASD). By combining the vapor deposition method and solution process, VASD conceptually inherits both advantages. A PbI_2 film is initially fabricated on the FFL by a solution process, and then it is reacted with the MAI vapor, leading to splendid crystallization and full coverage.[16] Recently, VASD has been further developed to operate under low pressure, showing shorter reaction time and lower MAI sublimation temperature.[28,29] In VASD, a one-dimensional, top-down reaction route was proposed for the diffusion-controlled, strongly temperature-dependent crystal growth:[30] (1) MAI initially reacts with the surface of the PbI_2 film, leading to the formation of perovskite crystal nuclei; (2) MAI gas molecules further diffuse into the inner PbI_2 region, inducing the growth of more perovskite crystals perpendicular to the substrate; (3) after the reaction, the perovskite grains merge together, and appear as larger grains.

2.2 Role of H_2O in perovskite film preparation

In the above methods, H_2O in various forms can affect the perovskite reaction process and the crystallization dynamics, leading to desirable or undesirable changes in the perovskite crystals as well as grains and even the morphology and bulk phase of the perovskite films, as shown in Fig. 3B. The mechanisms *via* which water in the preparation processes affects perovskite films will be discussed in the following sections.

2.2.1 H_2O in precursors. Most alkylammonium salts as well as some lead salts PbX_2 are hydroscopic, leading to the possibility that hydration water is added into the perovskite precursors and influences the formation of perovskite if the material is not stored in an inert atmosphere or is not dried very well before use.[31,32] Most recently, the hydration water in 3MAI:1Pb(Ac)$_2$·xH$_2$O (x = 1.5) in OSSD was proposed to combine with the new product $MAPbI_3$ in the DMF precursor, forming $MAPbI_3$·H_2O in the reaction (eqn (1) and (2)), benefiting the morphology and electronic properties of perovskite films by reducing surface roughness and the nonradiative pathways.[33] Following this work, further study demonstrated the optimized ratio 3MAI : 1Pb(Ac)$_2$·1.5H$_2$O, ascribed to the trade-off of reducing the non-radiative pathway and increasing porosity.[34] Similarly, the water of hydrate MAI, although it does not impact coverage, also lead to improved performance of PSCs by significantly enhancing the lifetime of excited carriers in the $MAPbI_3$ layer.[31]

$$3CH_3NH_3I + PbAc_2 \cdot 3H_2O \underset{\text{in solution}}{\overset{\leq 40\,^{\circ}C}{\rightleftharpoons}} CH_3NH_3PbI_3 \cdot H_2O + 2H_2O + 2CH_3NH_3Ac_2. \quad (1)$$

$$CH_3NH_3PbI_3 \cdot H_2O \xrightarrow{\text{in air}} CH_3NH_3PbI_3 + H_2O. \quad (2)$$

Moreover, a similar way of influencing the perovskite precursors is to directly add a small amount of liquid water into the solvents. The liquid water, unlike most uncontrolled hydration water, is accurately calculated and added into the perovskite precursors. For instance, 0–10% volume ratio of deionized water was added into the $MAPbI_{3-x}Cl_x$ perovskite precursors and the optimized 2 vol% water additive resulted in large grains with less voids in the morphology of the perovskite films, leading to a decrease in nonradiative trap states.[35] In this case, one possible influential mechanism is the formation of stable hydrates $MAPbI_{3-x}Cl_x$·nH_2O and a lower stabilization energy in the upcoming annealing step. Meanwhile, the changes of the physical and chemical thermodynamic properties of mixed solvents like boiling point, solubility, and vapor pressure, affect the orientation growth of the perovskite crystals.[35] Almost at the same time, another study also reported that the same volume of water was added into the perovskite precursor, but the changes in the films were minor and the device performances were influenced slightly (Fig. 5).[36] However, the different results in these two almost identical $MAPbI_{3-x}Cl_x$ experiments have not been further explained yet and we in passing point out that the underlying cause is likely the difference in the substrates since water molecules may disperse evenly on the more hydrophilic surface of PEDOT:PSS[35] compared with TiO_2,[36] so as to enhance the coverage of $MAPbI_{3-x}Cl_x$. However, further investigation is expected for the underlying mechanism. In recent publication, considering the coordination molecule competition, H_2O in the atmosphere is demonstrated to incorporate into the PbI_2:MAI:additive complex, competing with the solvent additive DMSO during crystallization of perovskite.[37] A balanced mole ratio of PbI_2 : MAI : additive complex (DMSO + H_2O) has been proposed to be 1 : 1 : 1.5,[37] yet the clear competition mechanism between H_2O and DMSO for coordination in the presence of DMF is not available.[37,38]

In parallel to the reports of water in OSSD precursors, one of the pioneering studies in two-step deposition was performed by Fu *et al.* who reported that 3PbAc$_2$·PbO·H_2O existed in the PbI_2 film when using Pb(Ac)$_2$·3H$_2$O as an ingredient, but the pure tetragonal phase $MAPbI_3$ nanostructure growth is unaffected based on the dissolution–recrystallization growth mechanism shown in Fig. 4B.[22] In addition, an appropriate amount of liquid water was shown to have a positive effect on the growth of perovskite by affecting the crystallinity of the PbI_2 film or participating in the growth of $MAPbX_3$.[39] A small amount of water has been used as an additive in PbI_2 DMF solution and MAI isopropanol solution respectively.[39,40] Both methods lead to larger grain size and better crystallinity, but the detailed mechanisms are not

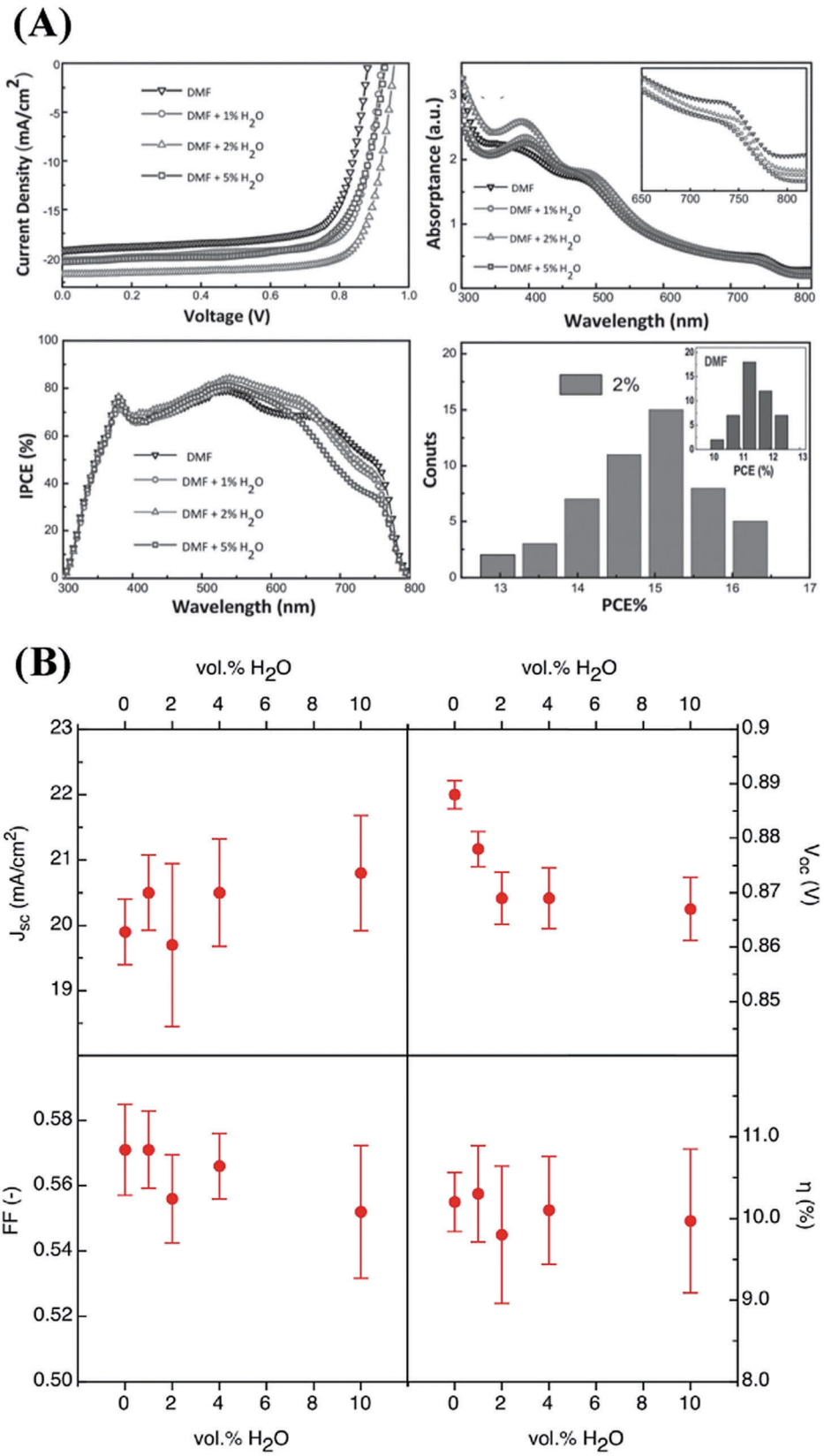

Fig. 5 Photovoltaic parameters of perovskite solar cells with active layers prepared from precursors with different water contents. (A) Reproduced from ref. 35, Copyright 2015 Wiley-VCH Verlag GmbH & Co. KGaA. (B) Reproduced from ref. 36 with permission from The Royal Society of Chemistry.

the same. Water in the PbI_2 solution modifies the properties of the H_2O/DMF mixed solvent, the PbI_2/PEDOT:PSS interface energy and the PbI_2 crystallinity, leading to a smooth, even PbI_2 film with the preferred (001) crystal plane parallel to the substrate.[39] Since perovskite crystals maintain the original orientation at the initial stage,[41] better PbI_2 crystallinity will be conducive to the perovskite film. In contrast, the water in the MAI solution is likely to assist the solid PbI_2 in reacting with the MAI, promote the crystallization of $MAPbI_3$ on the (110) plane and enlarge the grain size.[40] The increasing grain size might be explained by ingression of H_2O in the formation process, through hydrogen bonding interaction with $MAPbI_3$. It should be noted that a DMF solution could absorb water vapor. Clegg and his coworkers added controlled volumes of water into PbI_2/DMF solutions to simulate the role of ambient moisture, and found that an increasing concentration of water not only reduced the overall device performance but also exaggerated the scan-rate and directional-dependent hysteresis and introduce new transient behaviors. However, addition of water also improved the long-term device stability.[42] But this time the water amount added was two orders of magnitude lower than in the other reports,[39,40] and the device performance did not in this case fit the results of Wu *et al.*'s work.[39] Full understanding of the differences in the performance trends reported still needs further work, but could probably be linked to the discrepancies in the fabrication processes in a glove box and ambient environments.

2.2.2 H_2O in the spin-coating step. As mentioned above, the perovskite $MAPbI_3$ formation in OSSD involves nucleation and crystallization processes. According to the thin film growth theory and empirical data, a fast and high-density nucleation is expected so as to obtain better crystallization and surface morphology of the $MAPbI_{3-x}Cl_x$ film,[43] as supported by some studies using physical or chemical means to increase the number of nucleation sites.[44–46] Therefore, reducing the humidity directly leads to high supersaturation, and thus sidesteps island growth so as to heighten the coverage of the film.[43]

Nevertheless, unlike OSSD, moisture is more likely to participate in the reaction of PbI_2 film with MA^+ ions in the two-step spin-casting. Based on the interfacial reaction mechanism (Fig. 4A), compact $MAPbI_3$ covering PbI_2 hinders the 8 mg mL^{-1} MAI solution reacting with the inner PbI_2.[22] One solution is to prewet the substrate before spinning PbI_2 by controlling the exposure of the films towards moisture.[47] The 3 min exposure of mesoporous TiO_2 films to moisture resulted in more conversion of PbI_2 and in turn improved device efficiency, by virtue of the porosity of the PbI_2 film into which MAI could infiltrate more easily. We propose that water molecules may disperse discretely on the TiO_2 surface because of its poor hydrophilicity and then these in-site H_2O molecules attract PbI_2 by hydrogen bonds resulting in PbI_2 isolation, and thereby an increase in interspace is expected.

Also, moisture in the spin-casting process induces better reactions, larger grain size and better interconnectivity between perovskite crystals. Two mechanisms are responsible for the better perovskite crystallinity. For one, perovskite hydrates ($MAPbI_3{\cdot}H_2O$, $MA_4PbI_6{\cdot}2H_2O$ and $MAPbI_2Cl{\cdot}yH_2O$) appear as intermediates in or after spin-coating, which activate the reaction between PbI_2 and MAI, likewise with their intrinsic larger structural interspace providing extra fast paths for MAI diffusion.[48–50] The formation of $MA_4PbI_6{\cdot}2H_2O$ may be due to the coexistence of MAI and $MAPbI_3$ in the presence of excess water.[51] For another, moisture liquefies and ionizes the MAI, which exhibits more powerful capability of reacting with PbI_2.[48,49]

Nonetheless, increasing the relative humidity could greatly roughen the film surfaces, so it would to some extent cancel out the benefits of better crystallinity.[52] It is also noteworthy that methylammonium salts (MABr) liquefied in the moist air could not react with the PbI_2 and thus more MABr is required to ensure the complete chemical transformation of PbI_2 (see Fig. 6).[53] Balance of the effects is pertinent to the optimized range of R.H. but it appears to be very difficult since determination of the optimized R.H. is entangled with other parameters. Despite these issues, several groups have, respectively, used moisture (R.H. 30–60%) to drive the reaction of PbI_2 with MAI in the spin-casting process without a further thermal annealing step.[48,50,54] A dissolution and recrystallization mechanism at the perovskite grain edges is proposed.[54] Here, H_2O molecules are absorbed on the surface void states and grain edges, then destroy the bonding between MA^+ and the Pb–I cage. The released MA^+ then reacts with the Pb–I cage again after water evaporates, achieving void-free, larger crystalline films. Similar improvement is obtained by other solvent vapors, *e.g.* chlorobenzene for ambient engineering.[55] These successes offer a new platform, like using a room-temperature synthesis process to further reduce the costs of device fabrication and allow more acceptance.

2.2.3 H_2O in the annealing step. The thermal annealing process in solution deposition is an important step for the growth of $MAPbX_3$ crystals and the formation of polycrystalline perovskite films, accompanied by the evaporation of residual solvent. Meanwhile, by thermal annealing, the concern that water may get trapped in the structure units and affect the as-prepared perovskite films, is suggested to be dispelled.[56] In fact, a synergistic effect induced by a certain humidity and thermal annealing actually improves the perovskite film quality

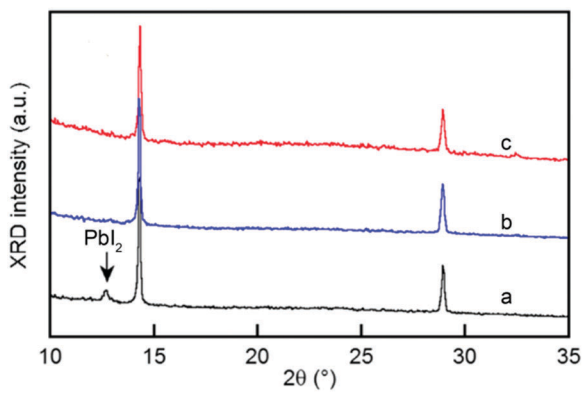

Fig. 6 XRD patterns of a MABr : PbI_2 solution with a molar ratio of either 1 : 1 in air (a) and an Ar-filled glovebox (b) or 1.2 : 1 in air (c); the down arrow indicates the position of the PbI_2 peak. Adapted from ref. 53 Copyright 2015, American Chemical Society.

and device properties. In 2014, Zhou and colleagues unprecedentedly annealed $MAPbI_{3-x}Cl_x$ films in a damp atmosphere (R.H. 30%), and consequently obtained larger crystal size and less nonradiative recombination.[13] A certain degree of moisture slows the crystal growth kinetic process by its effect on the solubility of the components and supersaturation of the perovskite, leading to a large grain size.[43,57–59] Also, a large crystalline grain structure and domain size in a moist environment is proposed to block the further ingression of water vapor.[60] $MAPbX_3$ ($X = I^-$, Br^-, Cl^-) crystals likewise coalesce to a larger size by the effect of water that modifies the grain boundaries, diminishing the number of defects.[57,61,62] This may be due to surface effects as well as lattice distortion that trigger the grain edges to be sensitive to moisture. The presence of small quantities of newly formed PbI_2 were later shown to benefit the electronic properties of grain boundaries in humid annealing, increasing the local conductivity through passivating traps at the grain boundaries and performing a self-doping role.[63] *In situ* techniques detected amorphous materials containing hydroxyl ions and the increase of grain size as direct evidence of the effect of water on $FAPbI_3$ films.[56,64]

Besides H_2O, the annealing process under different solvent vapors such as DMF and DMSO,[65] has resulted in better perovskite crystallinity. However, the mechanisms may be different. DMF and DMSO can dissolve PbI_2 and MAI as well as the $MAPbI_3$ film. The model by Liu *et al.*[61] proposed that the formation of a liquid or quasi-liquid phase on the surface and void area of the perovskite film by liquid phase sintering, may be responsible for film densification in the annealing process. An appropriate amount of H_2O in the organic solvent vapor is expected to enhance the surface solvation/dissolution of perovskite primary crystals, facilitating the integration and merging of initial perovskite crystals into larger grains and simultaneously healing the pinholes upon annealing.[66] In a humidified air annealing process, highly hygroscopic MA cations pull moisture from the environment. Water then partially dissolves the perovskite material and enlarges the $MAPbI_3$ crystals.[58] For a perovskite film spin-coated under low humidity and annealed under high humidity, a high nucleation density induced by high supersaturation appears in the spin-coating stage and causes layer growth of perovskite films, and the modest crystal growth under high humid conditions in the annealing stage can benefit the formation of perovskite films with better crystallinity and lower crystal defect density.[43] Meanwhile, MA vapor-involved annealing could also heal the perovskite film.[67] In this case well connected grains and less impurities were found,[67] which could be attributed to the potential formation of the $MAPbI_3{\cdot}xCH_3NH_2$ intermediate phase.[68,69]

However, the high humidity processing results in the appearance of more PbI_2 as insulating regions localized at the grain boundaries and within perovskite grains.[63] To restrain the likely adverse effects, the range of optimized R.H. had better be precisely controlled by considering other parameters like temperature scales, and ingredients. Regardless of the extremely humid conditions, annealing in a moderate humid atmosphere could be a self-improvement method for the perovskite device. Also, as many studies are continuously revealing the benefits that moisture induces in the annealing process in OSSD, it exhibits the capability of device fabrication under less restricted conditions.

The striking features like larger crystal size and less nonradiative recombination are still realized by post-treating perovskite films. Both the phenomena and essence are partially in common with the thermal annealing in a moist atmosphere. Defect density, mainly surface defects, decreases in accordance with less nonradiative decay after recrystallization of boundaries with or without thermal annealing.[70] Meanwhile, it is likely that MAI structurally becomes more mobile for better reacting with the remaining PbI_2 and excessive MAI could be removed as the result of being solubilized by water, both of which allow defects to be dispelled or filled in.[31] Very recently, Zhou *et al.* found deactivation of the perovskite surface under the effect of hydrogen bonds with uncoordinated iodide ions, like the deactivation by PCBM,[71] shifting the deep-level defects to shallow-level ones. Nevertheless, different from the long-term changes in other research studies, deactivation disappears after the escape of water vapor.

Concerning the incomplete reaction of MAI and PbI_2 in the fabrication, residual PbI_2 or MAI could be often expected. Recent studies revealed that the spatial distribution of remnant PbI_2 could affect the role of H_2O on $MAPbI_3$. Unreacted PbI_2, close to the substrate TiO_2, was reported to accelerate perovskite degradation during the exposure towards moisture[72] or the synergistic effect of moisture and illumination.[73] However, Petrus *et al.* found that the appearance rate of PbI_2 and monohydrate $MAPbI_3{\cdot}H_2O$ was slowed down with short-term exposure (R.H. 90%, <3 h).[74] They explained it with the passivation effect of PbI_2 at $MAPbI_3$ grain boundaries or terminations as Lei *et al.* did.[75] Interestingly, long-term exposure (R.H. 75%, 12 h) caused the same degradation degree between stoichiometric based devices and PbI_2-excess devices.[74] Although a full explanation is still lacking, it is possibly ascribed to substrates that affect the degradation degree,[73] which we will discuss in more detail in Section 3. In contrast, a MAI-enrich perovskite film, though it showed poor pristine performance, demonstrated improved electronic properties and better crystallinity after recrystallization in a humid atmosphere and a more stable energy output.[74]

2.2.4 H_2O in the whole solution deposition process. Very few reports study the influence brought by the changes of water in the whole solution deposition process. Lv *et al.* investigated the effect of H_2O and the assistance of solvents on the morphology of $MAPbI_3$ perovskite films and related device performances. By using DMAC as a solvent, they found that the most moderate humidity level is 28%.[76]

2.2.5 H_2O in or after vapor deposition. One of the pioneering works in VASD was done by Raga *et al.* who reported that H_2O could facilitate the reaction of CH_3NH_2 gas with the PbI_2 film.[77] With the aid of HI gas exposure, an ultra-smooth film was successfully formed under ambient air within several seconds and no high heating temperature was needed, as shown in Fig. 7.

Moisture plays the role of a trigger in the reactions. H_2O first induces PbI_2 to react with CH_3NH_2 (eqn (3)–(5)), then by

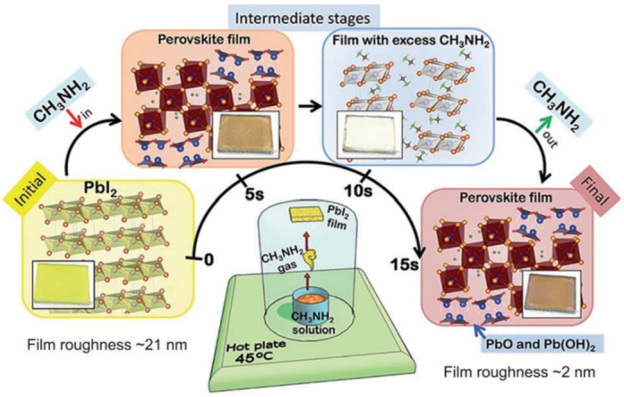

Fig. 7 Methylamine gas induced perovskite formation. Illustration of the setup used for processing perovskite at room temperature from simple precursors of CH_3NH_2 gas; the PbI_2 film is depicted in the lower middle part of the figure. Reproduced from ref. 77 with permission from The Royal Society of Chemistry.

HI vapor exposure, by-products PbO and $Pb(OH)_2$ convert to the initial reactant PbI_2 (eqn (6) and (7)).

$$3PbI_2 + CH_3NH_2 + H_2O \rightarrow 2CH_3NH_3PbI_3 + PbO, \quad (3)$$

$$CH_3NH_2 + H_2O \rightarrow CH_3NH_3OH, \quad (4)$$

$$3PbI_2 + 2CH_3NH_3OH \rightarrow 2CH_3NH_3PbI_3 + Pb(OH)_2, \quad (5)$$

$$PbO + 2HI \rightarrow H_2O + PbI_2, \quad (6)$$

$$Pb(OH)_2 + 2HI + H_2O \rightarrow 2H_2O + PbI_2. \quad (7)$$

Patel *et al.* exhibit the effect of ambient air (R.H. 40 ± 10% at 21 ± 1 °C) after the two-step thermal evaporation process.[78] In analogy to the effect of moisture as mentioned in OSSD and SSD, water vapor exposure makes unreacted MAI mobile, thereby facilitating chemical transformation of PbI_2 to $MAPbI_3$. Intermediate dihydrate $MA_4PbI_6{\cdot}2H_2O$ was also detected, and it consumed excess MAI and favored $MAPbI_3$ growth (Fig. 8).

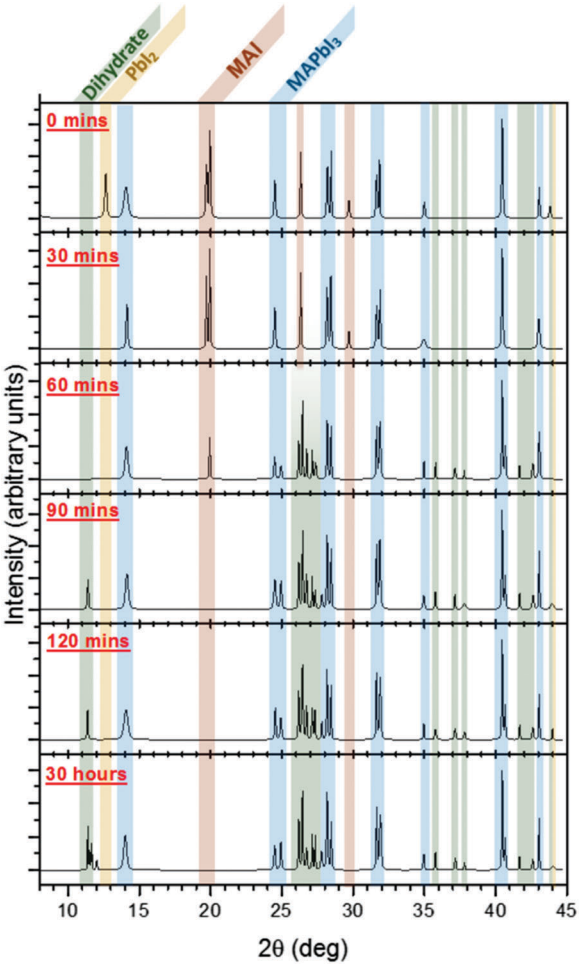

Fig. 8 X-ray diffraction patterns following the evolution of $MAPbI_3$ from the initial bilayer MAI/PbI_2 films (0 min), to the nascent perovskite (30 min), and then finally to the $MAPbI_3$ film (90 min). After 90 min, the dihydrate $MA_4PbI_6{\cdot}2H_2O$ is observed to form (2θ = 11.4°, 11.5°, and 11.6°). Reproduced from ref. 78, Copyright 2015, American Chemical Society.

3. H_2O in the perovskite crystal and film

3.1 Effect of H_2O on perovskite composition

A crucial question raised is what intermediates and products are responsible for the decay of the perovskite films caused by moisture. To answer this question, $MAPbI_3$ films on various substrates are generally exposed to carefully controlled environmental conditions and exposure times.[11,79–81] Despite some existing discrepancies, an apparent conclusion is that water plays a catalytic role in the whole degradation process, thereby speeding up the decomposition of perovskite. A conclusive $MAPbI_3$ degradation reaction solely affected by water is shown in eqn (8).

$$CH_3NH_3PbI_3 \overset{H_2O}{\rightleftharpoons} CH_3NH_3PbI_3 \cdot H_2O, (CH_3NH_3)_4PbI_6 \cdot 2H_2O \rightarrow PbI_2 + \text{other compositions}. \quad (8)$$

Nevertheless, a large number of degradation routes and decomposed products, summarised in Table 1, have been proposed in each specific circumstance and some are quite different, even just slightly modulating the exposed conditions.

Firstly, for identifying the intrinsic stability of perovskite, $MAPbX_3$ is either placed in a dry N_2 atmosphere or under vacuum conditions. In this duration, perovskite films have a negligible degradation except with other treatments like light illumination and high temperature,[82,83] consistent with the recent acknowledgement that light-activated oxygen degradation and thermal effects have substantially key roles in the degradation process.[84–86] Deretzis *et al.* proposed two possible degradation mechanisms for the degradation under air and vacuum conditions (Table 2):[87] (1) chemical degradation involving the catalyst role of water; (2) thermodynamic degradation through the creation of volatile molecular defects even partially occurring under vacuum. Following this work, Alberti *et al.* found that $CH_3NH_3PbI_3$ goes through a similar degradation dynamics pathway, beginning with a phase change from tetragonal to

Table 1 Summary of degradation products of perovskites in different environments

Composition	Atmosphere	Conditions[d]	Sub[a]	Degradation products	Ref.
$CH_3NH_3PbI_3$	In vacuum	10^{-2} Torr	TiO_2	C-FP[b]: PbI_2	87
	In situ ambient atmosphere[e]	60% R.H. + in the dark + R.T.			
	In vacuum	9.3×10^{-5} kPa	TiO_2	C-FP: PbI_2 and no hydration	88
	In situ ambient atmosphere	60% R.H. + R.T.			
	In situ humid atmosphere[f]	50 ± 5% R.H. + in the dark + 23 ± 1 °C	Al_2O_3	NA	89
		90 ± 5% R.H. + in the dark + 23 ± 1 °C		C-FP: hydration, possible $(CH_3NH_3)_4PbI_6{\cdot}2H_2O$ and no PbI_2	
	In situ humid atmosphere[g]	15% R.H. + in the dark + R.T.	FTO	NA	91
		30% R.H. + in the dark + R.T.		C-I: PbI_2 crystal, MAI crystal	
		60% R.H. + in the dark + R.T.		C-FP: PbI_2 crystal, MAI amorphousness	
	N_2 with moisture flow	80 ± 5% R.H.	FTO	C-I[c]: $CH_3NH_3PbI_3{\cdot}H_2O$ C-FP: PbI_2(s) and CH_3NH_3I (aq.)	90
	N_2 with moisture flow	80% R.H.	PEDOT:PSS	C-I: $CH_3NH_3PbI_3{\cdot}H_2O$ C-FP: $CH_3NH_3PbI_3{\cdot}H_2O$, $(CH_3NH_3)_4PbI_6{\cdot}2H_2O$ and in the dehydration, PbI_2	93
	N_2 with moisture flow	20% R.H. + 22.9 ± 0.5 °C	Glass	NA	81
		50% R.H. + 22.9 ± 0.5 °C		C-I: PbI_6^{4-} compounds C-FP:PbI_2 and dihydration, possible $(CH_3NH_3)_4PbI_6{\cdot}2H_2O$	
		80% R.H. + 22.9 ± 0.5 °C			
		98 ± 2% R.H. + 22.9 ± 0.5 °C			
	Compress filtered air with moisture flow	80 ± 5% R.H.	Glass	C-I: $CH_3NH_3PbI_3{\cdot}H_2O$ and $(CH_3NH_3)_4PbI_6{\cdot}2H_2O$ C-FP: $(CH_3NH_3)_4PbI_6{\cdot}2H_2O$ and PbI_2	94
	Ambient air flow	60% R.H. + $h\nu$ + 35 °C	TiO_2	C-FP: PbI_2(s) and I_2(s)	11
	Ambient air flow	25% R.H. + 24.7 °C	Au/Si	C-FP: amorphous C remain and PbI_2(s)	104
	O_2 flow	Pure O_2 gas	Au/Si	NA	79
	Ambient air flow	41% R.H. + 21 °C + 1 atm		C-FP: PbI_2, hydrocarbon complex and O	
		21 °C + low pressure		at the exposure $>2 \times 10^{10}$ L	
	H_2O vapor flow	Pure H_2O vapor			
	Ambient air flow	40 ± 5% R.H. + $h\nu$	ZnO/Si	C-FP: $(CH_3NH_3)_4PbI_6{\cdot}2H_2O$ and PbI_2	97
		75% R.H. + $h\nu$			
	Ambient air flow	24 ± 2% R.H. + $h\nu$ (0.25–0.5 mW cm^{-2}) + 25 ± 1 °C	FTO	C-I: PbI_{2+x}^{x-} compound C-FP: $PbCO_3$, $Pb(OH)_2$, PbO and no PbI_2	95
$CH_3NH_3Pb(I_{1-x}Br_x)_3$ $(0 < x < 1)$	Ambient air flow	67 ± 5% R.H. + $h\nu$ (500–2000) + 27 ± 1 °C	FTO	C-FP: PbI_2, $CH_3NH_3PbBr_3$	80
		67 ± 5% R.H. + $h\nu$ (50–100lx) + 22 ± 1 °C		C-FP: PbI_2, $CH_3NH_3PbBr_3$	
		67 ± 5% R.H. + in the dark + 22 ± 1 °C		C-FP: $CH_3NH_3Pb(I_{1-y}Br_y){\cdot}3H_2O$ $(y < x, 0 < x < 0.3)$ and PbI_2	

[a] Substrate. [b] C-FP, confirmed final products. [c] C-I, confirmed intermediates. [d] Conditions include relative humidity, light irradiation, temperature and pressure in this order. [e] Films are placed under an undisturbed, natural humid atmosphere. [f] The humidity was achieved by a water/glycerol solution with control of the water to glycerol ratio. [g] Films are placed in a glovebag with a humidifier and a hydrometer.

cubic phase with no hydration taking place.[88] Water was just suggested to speed up the intrinsic thermodynamic mechanism by transferring the proton of MA^+ to I^- and releasing CH_3NH_2.

Furthermore, several investigations have presented the performance of perovskite materials in an artificially sealed humid environment. Christians *et al.* found sole formation of $MA_4PbI_6{\cdot}2H_2O$ without detecting PbI_2 following exposure to an artificially airtight humid atmosphere created by a water/glycerol solution.[89] Likewise, Zhao *et al.* reported that $MAPbI_3$ powder was fully recovered if no loss of PbI_2 and MAI occurred after drying liquid water.[90] Moreover, a very recent study exhibited that an *in situ* humid atmosphere causes crystalline MAI to become an amorphous phase without breaking its bonding structue.[91] These groups all reported no loss of MAI following the sealed humid air exposure treatment. However, Lin *et al.* observed that in a sealed deuterium oxide (D_2O) atmosphere, the decomposition of $MAPbI_3$ was initialized by vaporization of CH_3NH_2, accompanied by quick formation of the PbI_2 phase.[92] Fig. 9 provides a view of the ion distributions from 3D perspectives as exposure time increases.[92] Flowing moist inert gas also accelerates the hydration of perovskite and facilitates the irreversible decomposition towards PbI_2 *via* evident phase separations.[90]

However, no matter whether perovskite films degrade in a sealed humid atmosphere or exposed to flowing moist inert gas, the decomposition rate of perovskite crystals is substantially related to the exposure degree towards R.H.[81,93] High R.H. like 80–100%, represents short exposure time and fast transfer to hydration and PbI_2. Yang *et al.* proposed $\tau_{1/2} \approx$ 4–34 h for the

Table 2 Summary of the impacts of water in the fabrication steps on the performance of PSCs

Methods	Involving steps	Forms	Device configuration	J_{sc} (mA cm^{-2})	V_{oc} (V)	FF	PCE (%)	Ref.
OSSD	Ingredient	3CH_3NH_3I: 1$PbAc_2$·1.5H_2O hydration	ITO/PEDOT:PSS/P[a]/$PC_{61}BM$/C_{60}/BCP/Ag	20.6 (19.6)	0.865 (0.749)	0.71 (0.65)	12.3 (9.3)	33
	Precursors	2% H_2O + DMF precursor	ITO/PEDOT:PSS/P(Cl)[b]/$PC_{61}BM$/BCP/Ag	20.8 (19.0)	0.95 (0.87)	0.78 (0.73)	15.0 (11.6)	35
		2% H_2O + DMF precursor	ITO/c-TiO_2[c]/P(Cl)/P3HT/Au	19.7 (19.9)	0.869 (0.888)	0.558 (0.570)	9.7 (10.2)	36
	Spin-coating	Moisture R.H. = ~70%	ITO/c-TiO_2/meso-TiO_2[d]/P(Cl)/Spiro-OMeTAD/Ag	12.0 (19.5)	0.41 (0.82)	0.447 (0.525)	2.2 (8.4)	43[e]
	Annealing	Moisture R.H. = ~35%	ITO/PEDOT:PSS/P(Cl)/$PC_{61}BM$/BCP/PCN/Ag	19.9 (19.0)	0.99 (0.86)	0.78 (0.75)	15.4 (12.3)	57
	Post annealing	4 h exposed in R.H. = ~35% at R.T. after annealing	ITO/c-TiO_2/P(Cl)/Spiro-OMeTAD/Au	18.5 (17.5)	0.90 (0.85)	0.57 (0.55)	9.4 (7.9)	31
	Whole process	Moisture R.H. = ~28%	FTO/c-TiO_2/P/Spiro-OMeTAD/Ag	21.4 (19.6)	1.07 (1.05)	0.668 (0.711)	15.3 (14.6)	76[e]
SSD	Precursors	2 wt% H_2O[f] + PbI_2 DMF	ITO/PEDOT:PSS/P/$PC_{71}BM$/BCP/Ca/Al	20.8 (0.329)	1.001 (0.10)	0.82 (0.19)	17 (~0.0)	39
		5 vol% H_2O[g] + MAI IPA	ITO/c-TiO_2/meso-TiO_2/P/Spiro-OMeTAD/Ag	22.06 (20.41)	0.97 (0.89)	0.54 (0.50)	11.74 (9.25)	40[e,i]
		2 mol% H_2O[h] + PbI_2 DMF	ITO/PEDOT:PSS/P/$PC_{61}BM$/BCP/Ca/Al	0.88 (0.98)	10.60 (14.58)	0.67 (0.73)	6.2 (10.4)	42
	Spin-coating	10 min exposed in R.H. = ~40% at R.T. after spin-coating	ITO/ZnO/P/P3HT/Ag	16 (12)	0.94 (0.88)	0.57 (0.44)	9 (4.6)	48
		R.H. = ~40% in spin-coating MAI layer	ITO/c-TiO_2/meso-TiO_2/P/Spiro-OMeTAD/Au	17.39 (17.87)	0.997 (0.995)	0.74 (0.72)	12.8 (12.7)	49
		60 min exposed in R.H. = 36–43% at R.T. after Spin-coating	ITO/c-TiO_2/meso-TiO_2/P/Spiro-OMeTAD/Ag	21.38 (18.66)[j]	1.00 (0.88)[j]	0.76 (0.79)[j]	16.2 (12.8)[j]	54[e]
VASP	In the vapor deposition	Atmospheric water vapor	ITO/c-TiO_2/meso-TiO_2/P/Spiro-OMeTAD/Ag	19.0 (—)	1.04 (—)	0.69 (—)	13.5 (—)	77

The values of device performance in the table are average values if they are not specially noted. Parenthesis represents the controlled groups in which water is absent. [a] P: $MAPbI_3$ perovskite. [b] P(Cl): $MAPbI_{3-x}Cl_x$; perovskite. [c] c-TiO_2: compact TiO_2 layer. [d] Meso-TiO_2: mesoporous TiO_2 layer. [e] Not average value. [f] (wt% *vs.* DMF). [g] (vol% *vs.* IPA). [h] (mol% *vs.* PbI_2). [i] Reverse scan. [j] Thermal annealing results.

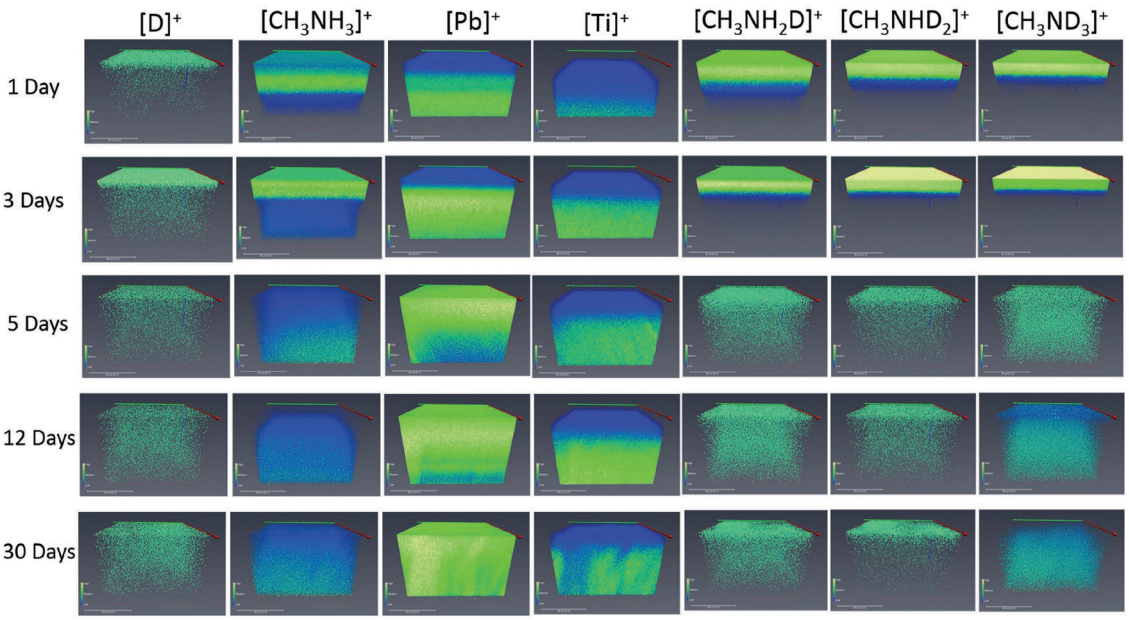

Fig. 9 3D reconstructed images of deuterium, methylammonia, PbI_2, and TiO_2 at different exposure times. Color map illustrating the molecular density from high (bright green) to low (blue). Reproduced from ref. 92, Copyright 2017 Wiley-VCH Verlag GmbH & Co. KGaA.

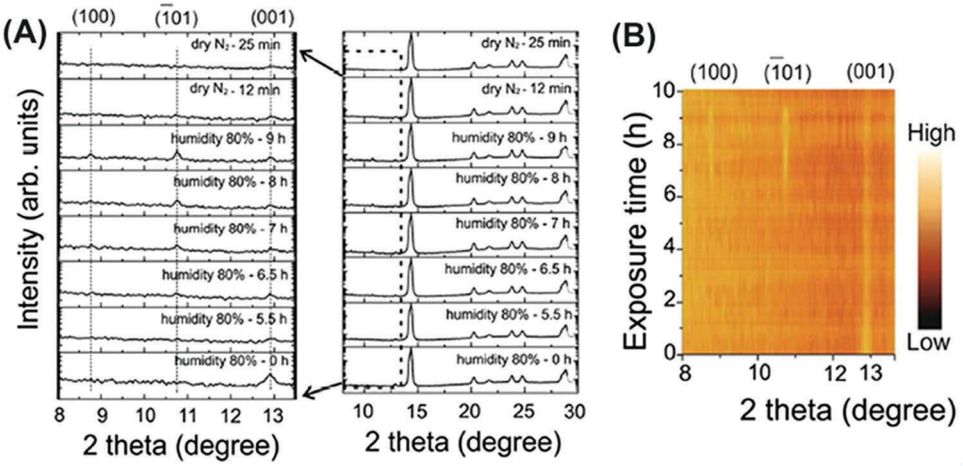

Fig. 10 (A) Time-resolved *in situ* XRD of a $MAPbI_3$ film during the first hydration–dehydration round and a zoomed-in image at 2θ angles from 8.0° to 13.5°. (B) The corresponding contour plot showing changes in XRD peak intensity during the first hydration–dehydration cycle. Reproduced from ref. 93, Copyright 2016 American Chemical Society.

decomposition rate of a perovskite film in 80–98% R.H., whereas it can reach up to 10 000 h if R.H. is 20%.[81] To identify the starting point of perovskite decomposition with structure changes, Li *et al.* proposed a reaction threshold $>2 \times 10^{10}$ L H_2O exposure (one L is equal to 10^{-6} Torr s).[79] After reaching a certain degree of water molecules *via* exposure towards moisture for a certain time, in most studies perovskite intermediates will appear in the form of reversible hydration phases $MAPbI_3{\cdot}H_2O$ and $MA_4PbI_6{\cdot}2H_2O$. Lots of studies have reported that dry N_2 or low humid air encourages the back reaction of perovskite hydration (Fig. 10).[93,94] Further irreversible decompositions present the separate appearance of porous and distorted hexagonal PbI_2 platelets in the film.[95,96]

Given that the working PSCs in actual situations are contemporaneously under direct exposure to light, heat, water *etc.*, the coupled effects of moisture with other environmental factors on $MAPbI_3$ should also be considered. Studies presented that the cooperative effects of water with light, ambient air and high temperature would aggravate the water-induced influence.[11,95,97–99] In these cases, many groups revealed that deterioration of perovskite films could occur at lower R.H. with different degradation pathways and final products (Table 1). For instance, Shirayama *et al.* recently indicated that two competing ways, perovskite hydration and the formation of a PbI_2 phase, occurred spontaneously under the cooperative effect of ambient air flow (R.H. 40%) and light.[97] Niu *et al.* reported that humid air with oxidization of oxygen and light illumination induced decomposition of MAI by losing I in gaseous form or solid I_2,[11] as did Dao *et al.*,[100] partially due to the deprotonation effect of O_2 in the trapped charge-induced $MAPbI_3$ degradation mechanism.[101] Furthermore, the Pb solid remnant was found as PbO, $PbCO_3$, $Pb(OH)_2$ and other forms (Table 1 and eqn (9)–(13)) when the decomposition involved CO_2 and O_2.[95,102] Also, Ruess and colleagues found that the coupled effects of illumination and moisture led to segregation of the mixed halide to $MAPbI_3$ and $MAPbBr_3$ in $MAPb(I_{1-x}Br_x)_3$ followed by the appearance of PbI_2 *via* decomposition of $MAPbI_3$.[80] Very recently, a new phase PbI(OH) was reported due to the transformation of PbI_2 at the interface of the perovskite and Spiro-OMeTAD after continuous illumination and moisture exposure (R.H. 60%).[103] An additional solid remnant, amorphous C, is observed on Au coated Si wafers.[79,104] The appearance of this hydrocarbon layer may be due to the interaction of low-energy electrons with $MAPbI_3$ by initially triggering the breakdown of C–N bonds.[105] Besides, it is probably instead that the unique carbon solid comes from the catalyst of Au under light irradiation. Electrons gain their own energy which is enough to activate the MA^+ group.[106,107] Beyond the obscure solid remnant, the probing of $MAPbI_3$ decomposition involves puzzling gaseous products. The existence of gaseous products has been confirmed by the bubbles at the interface of the Al electrode,[108] whereas gaseous components deriving from CH_3NH_3I are not unveiled yet and speculated to be diverse species, *e.g.* I_2, HI, CH_2NH_2, NH_3, and H_2.[11,79,95] In future work, characterization and analyses of the gaseous products are expected to pave the way for overall understanding of the perovskite decompositions.

$$4CH_3NH_3PbI_3 + 8H_2O \rightarrow (CH_3NH_3)_4PbI_6{\cdot}2H_2O + 3(OH)_2 + HI\uparrow \quad (9)$$

$$(CH_3NH_3)_4PbI_6{\cdot}2H_2O \rightarrow (CH_3NH_3)_xPbI_{2+x} + (4-x)CH_3NH_2\uparrow + (4-x)HI + 2H_2O \quad (10)$$

$$2(CH_3NH_3)_xPbI_{2+x} + 2CO_2 + O_2 \rightarrow 2PbCO_3 + 2I_2\uparrow + 2xCH_3NH_2\uparrow + 2xHI\uparrow \quad (11)$$

$$(CH_3NH_3)_xPbI_{2+x} + H_2O + \frac{1}{2}O_2 \rightarrow Pb(OH)_2 + I_2\uparrow + xHI\uparrow + xCH_3NH_2\uparrow \quad (12)$$

$$Pb(OH)_2 \rightarrow PbO + H_2O \quad (13)$$

3.2 Effect of H_2O on perovskite structure

The ingression of water is found to initially chemisorb on a particular $MAPbI_3$ region, extracting electrons from the perovskite surface like a p-type dopant.[79,109] Grain boundaries substantially

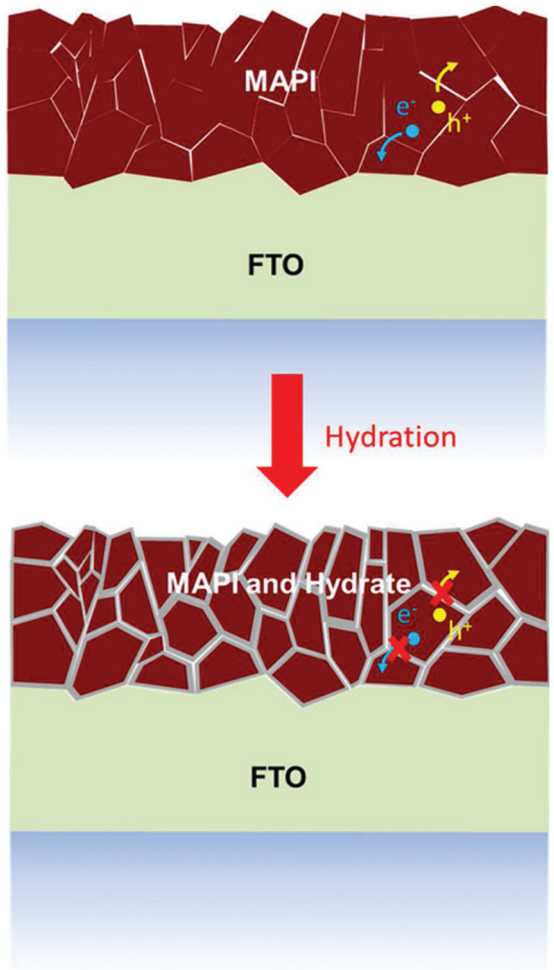

Fig. 11 Microscopic degradation model of MAPI thin films under partial hydration. Reproduced from ref. 94, Copyright 2015 American Chemical Society.

exist in the polycrystalline perovskite films and their role in the immigration of water attracts lots of attention. Both calculations and experiments indicated that the grain boundaries and defects pave the way for the embedment of absorbed H_2O molecules, yielding a structural decomposition for $MAPbX_3$,[94,110,111] as shown in Fig. 11, while new grain boundaries are generated in this duration.[93] Chiang *et al.* proposed that pinholes and defects produced by light and heat within the grain boundaries could explain the phenomenon that large grain size is conducive to the long-term stability with or without moisture.[112] At the same time, Wang *et al.* found that an amorphous perovskite region exists between the perovskite grains, responsible for the quick water ingression parallel to the substrate, further emphasizing the significance of increasing grain size and improving grain boundary qualities.[113] In addition, trapped charge along grain boundaries is demonstrated to stimulate the irreversible deterioration in moisture-induced degradation.[101] A local electric field is assumed to deprotonate the organic cations by transferring the proton onto neutral H_2O molecule, releasing volatile compound CH_3NH_2 or $HN{=}CHNH_2$, similar to the early acid–base mechanism proposed by Frost *et al.*[114]

Through investigating the crystal surfaces of as-grown and degraded $MAPbBr_3$ perovskite single crystals, Murali *et al.* revealed that high humidity would restructure the crystal surface by surface hydration, yielding polycrystalline structures and grain boundaries.[115] Grancini *et al.* reported that the perovskite single crystal edge is more sensitive to moisture, where hydrogen bonding occurs spontaneously between water molecules and the perovskite lattice, assumed as the first step of the hydration process.[116]

Further permeation of water into the inner structure of the perovskite is proposed to be related to the perovskite lattice, also determined by their different terminations (MAI-terminated and PbI-terminated) and the polarities.[110,117,118] The immigration can occur very fast within a few seconds at low R.H. with no obvious change appearing in optical absorption and structure.[119] In the (001) surface, the MAX-termination, although structurally more stable than the PbX_2-termination,[120,121] presents ~0.3 eV absorption energy of water with the large inner structural space, implying that water molecules can move freely with almost no constraint.[118] The MAI-terminated surface may experience a quick decomposition called a solvation process.[110] Iodide atoms, as shown in Fig. 12A, are replaced by water molecules, bonding with the MA molecules and escaping in the form of MAI molecules,[110] similar to the super alkali halide crystal model proposed by Fang *et al.*[122] In the case of a PbI_2-terminated (001) surface, no solvation process happened due to the shorter and stronger Pb–I bonds.[110] Instead, water molecules directly went into the perovskite crystal structure due to the decreased energy in the diffusion and large interspace in the lattice structure, finally taking up a position in the perovskite slab (Fig. 12B). Another simulation recently indicated that the existence of O_2 could induce higher H_2O molecules adsorption on the PbI_2-terminated surface, further confirming the synergistic effects of H_2O and O_2.[99] Furthermore, water adsorption is also investigated on other perovskite surfaces. Zhang *et al.* revealed that in the (110) surface, hydroxyl groups and hydroxyl radicals

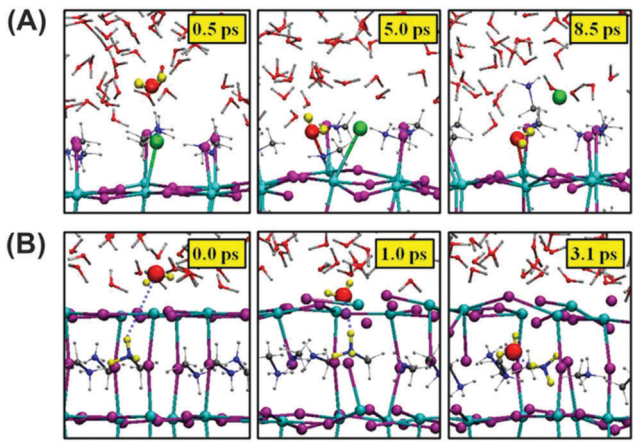

Fig. 12 (A) Nucleophilic substitution of a surface iodide atom by a water molecule in the MAI-terminated $MAPbI_3$ slab. (B) Incorporation of a water molecule to the PbI_2-terminated slab. Adapted from ref. 110, Copyright 2015 American Chemical Society.

rather than H_2O molecules are responsible for the quick deprotonation of MA,[102,123] in accordance with an ordinarily fast decomposition caused by the remaining hydroxyl radicals and hydroxyl groups in contact with the ZnO/perovskite interface.[124] Lv and colleagues showed that the erosion of water on single crystal $MAPbI_3$ is slower both in (100) and (112) facets but not in the (001) facet, attributing the different erosion rates to local atom arrangements.[125]

Humidity-induced phase transitions in many studies include the formation of perovskite hydration compounds ($MAPbI_3{\cdot}H_2O$ and $MA_4PbI_6{\cdot}2H_2O$) with the structure homogenously changing from 3D $MAPbI_3$ crystals to $MAPbI_3{\cdot}H_2O$, a 1D structure and $MA_4PbI_6{\cdot}2H_2O$, a 0D network (Fig. 13),[94,126] with the column of the perovskite unit cells swelling,[94,127] which may lead to lattice stress and eventually polycrystalline films. Detailed analysis manifested that $MAPbI_3$ crystals experience a space group transformation, derived from a change of hydrogen bonds between the MA^+ cation and I atoms after H_2O insertion.[128] Likewise, new hydrogen bonds are proposed to be established between the O of H_2O and H in NH_3 as well as between H in water and halide anions.[127] It should be noted that not all reports confirmed the generation of $MA_4PbI_6{\cdot}2H_2O$,[90,103] which may be due to the different perovskite phase, α phase and β phase, with change of the I–Pb–I bond angle.[103] Although the back reaction can occur under low R.H. conditions, structural changes including destruction of the original long range order and porous microcrystal solid, caused by dihydration, are still commonly found in the microstructure.[93,129–131] The decomposition of the perovskite is accompanied by a change in film thickness.[94,97]

3.3 Effect of H_2O on perovskite properties

Keeping in mind that the water molecules chemisorbed on the film surface extract electrons, the valence band maximum (VBM) and conduction band minimum (CBM) of the $MAPbI_3$ are shifted towards lower values.[79] Further evidence is the declining resistance of the $MAPbI_3$ films following the power law distribution in moisture, proposed to exhibit p-type conduction.[109] Nonetheless, chemisorbed water does not evidently change the bandgap (E_g), partially because the water molecules do not chemically react with the perovskite surface but interact electrostatically.[79] In addition, water molecules on the perovskite surface were revealed to reduce deep electron traps as well as to slow down the recombination rate.[132] But more substantial lattice distortion in the crystal edge is also reported, widening the local bandgap along with faster carrier recombination.[116] Another study showed that aged single crystal surfaces and polycrystalline films both obtain similar carrier lifetime and band gap, but poorer than crystal bulk.[115]

Lately, lattice surface hydration has been found to improve the local bandgap of MAI^- exposed crystals by a very small value by the slight upshift of the CBM, whereas water expands the bandgap of PbI_2-terminated slabs by ~0.30 eV.[110,118] Also, the optical proprieties are unchanged when the water absorbs on the MAI^- surface. However, after H_2O pierced into the inner space, the local bandgap increased from ~1.6 eV to 3.1 eV

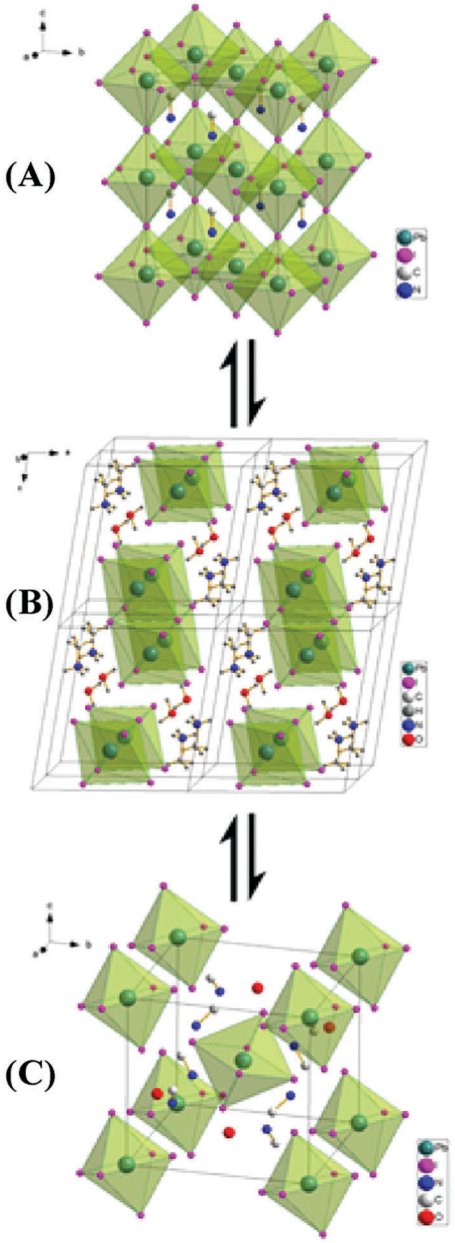

Fig. 13 (A) Structure of $MAPI_3$ in its cubic phase. (B) Structure of the monohydrate phase, $MAPbI_3{\cdot}H_2O$. (C) Structure of the dihydrate, $MA_4PbI_6{\cdot}2H_2O$. Adapted from ref. 94, Copyright 2015 American Chemical Society.

(hydrated perovskite) and finally became 2.4 eV (PbI_2 remnant).[83,94] Another indication of the decomposition of $MAPbI_3$ is the striking color change from dark brown to yellowish, in agreement with the remaining absorption <525 nm.[11,95,96] The hydrated layers are proposed as insulators to block the transport of carriers and thereby instigate more recombination of electrons or holes.[94] Recently, Long *et al.* reported that the acceleration of electron–hole recombination can be attributed to the high-frequency polar vibrations of water.[132] Irreversible decomposed product PbI_2 caused by water exposure is found to spatially contaminate the conductivity within the grain inner regions and grain boundaries.[63]

4. H_2O at interfaces between perovskite films and functional layers

Thus far, we have concluded how water impacts intrinsic perovskite films. Furthermore, another key factor, interfaces between perovskite and other functional layers, has been recently pointed out to immeasurably affect the device lifetime.[89,108,133–135] To investigate the relationship between interfaces and moisture, the FFL and SFL will be paid special attention.

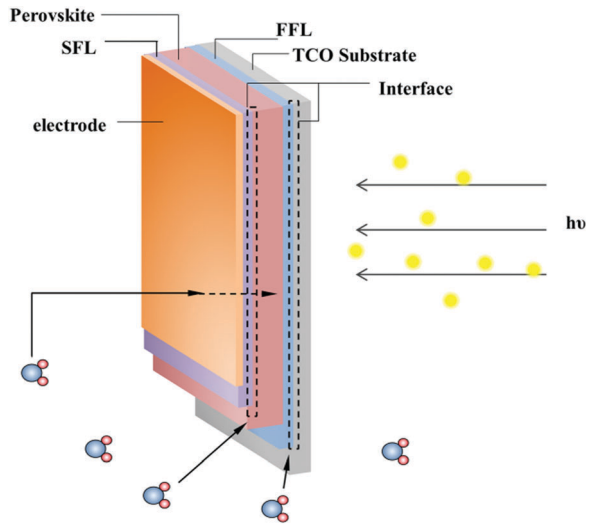

Fig. 14 Two kinds of pathways for intrusion of H_2O molecules.

The nanostructure and nature of the FFL play unignorable roles in the water-induced interfacial degradation (Fig. 14).[131,136] The electron selective TiO_2 layer in n–i–p type cells may improve moisture resistance *via* helping the perovskite to better crystallize,[131] and further change the degradation degree by manipulating its intrinsic nanostructure.[136] In contrast, electron selective material ZnO in n–i–p cells, hole transport material PEDOT:PSS in p–i–n cells and insulating material Al_2O_3 define themselves with hydrophilic qualities as accomplices in the intrusion of moisture.[136–138] The increase of the broad peak of O–H stretching in FTIR after exposure to water shows that the hygroscopic Al_2O_3 film induces the water in air to ingress in the form of droplets.[136] IR also reveals that an acid–base reaction occurs at the contact of ZnO with NH_3^+ groups of methylammonium cations.[136] Hydroxyl groups and acetate ligands are often kept on the ZnO particle surfaces and accelerate the transformation of $MAPbI_3$ to PbI_2 especially when the ZnO/perovskite structure is kept in a high temperature, consistent with theoretical simulations (Fig. 15).[123,124,139]

Besides, another reason could be the more basic surfaces of ZnO compared with those of TiO_2 or ITO, which would facilitate protons to transfer and produce methylamine.[124,137] Also, an aqueous solution of ZnI_2 was proposed by Dkhissi *et al.* to

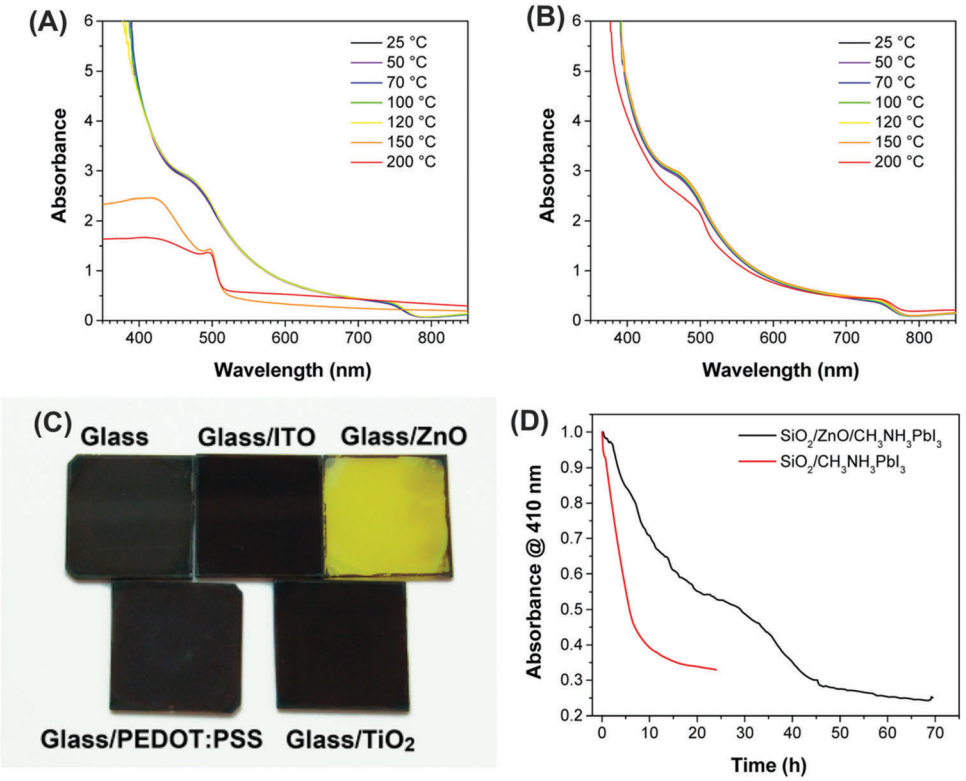

Fig. 15 Absorbance spectra of $MAPbI_3$ films deposited on different substrates. (A) ITO/ZnO or (B) ITO substrates and annealed at various temperatures for 5 min. (C) Photograph of $MAPbI_3$ films on various substrates after heating to 100 °C for 20 min. (D) Normalized absorbance at 410 nm as a function of time for SiO_2/ZnO/$MAPbI_3$ and SiO_2/$MAPbI_3$ films exposed to 98 ± 2% R.H. Reproduced from ref. 124, Copyright 2015 American Chemical Society.

probably exist in this degradation.[137] But in one case, a small amount of PbI_2 at the perovskite surface and interface with ZnO, derived from high humidity treatment, was proposed to remarkably slow down the degradation of PSC performance, and contribute to the difference in chemical kinetics.[75]

Capping functional layers and their contact interface with perovskite are other aspects that impact the moisture-induced aging (Fig. 14). Although Li-TFSI doped Spiro-OMeTAD is well-known for its hydrophilicity,[81,140] few studies explored the detailed reason for this until Song *et al.* recently proposed that the moisture-invoked degradation at the interface is inhomogeneous, and assumed that the spontaneous existence of severe hydration and repression of recombination centers was induced by uneven distributed H_2O and MAI in the Spiro-OMeTAD film.[131] Besides Spiro-OMeTAD, *in situ* experiments showed that PCBM in inverted PSCs absorbed water and deteriorated perovskite from the interface.[108,141,142] In a recent investigation, Zhao and colleagues directly contacted an Al electrode with perovskite and found that the first step for $MAPbI_3$ degradation is the redox reactions at the interface proceeded by moisture-driving ion migrations.[143] They also pointed out the importance of seeing the PSCs as a whole for discussing stability issues. Also, the Au electrode was used to slow down the release rate of trapped H_2O molecules, based on the longer remaining time of the dihydrate phase.[144]

5. Influence of H_2O on PSC performance and stability

The influence of H_2O on perovskite films during processing and the underlying mechanisms were discussed with further discussion in Section 2. A certain amount of water can improve perovskite film quality in most fabrication cases, which could also enhance the PSC performance. We have summarized this in Table 2.

The power conversion efficiency (PCE) is an important parameter to evaluate the initial performance of solar cells, which depends on the short-circuit current J_{sc}, open-circuit voltage V_{oc} and fill factor FF. J_{sc} is generally determined by the bandgap, light absorption and carrier lifetime/diffusion length. The bandgap is an intrinsic material property and irrelevant to perovskite film quality. More surface coverage and thicker active layer can increase the light absorption. It is reported that H_2O in the solution fabrication enhances the efficiency of light absorption,[33,40,76] partially due to improved coverage.[35,76] Nevertheless, ambient water vapor in the spin-coating step in OSSD obviously reduced the coverage of the $CH_3NH_3PbI_3$ film, thus leading to a poor J_{sc} originating from the high transmittance and low absorption of light.[43] In some cases, the carrier diffusion length and carrier lifetime is long, contributing to efficient carrier collection,[54,59] which could be considered as the result of smooth surface,[33] better crystallinity,[76] and reduced grain boundaries.[48]

V_{oc} mainly depends on the recombination pathways, especially nonradiative recombination centers in the solar cell. The trap states are often generated by poor quality of the perovskite films. Water in synthetic stages could reduce the trap states in boundaries,[31,40,54] and promote crystallinity[54] to ensure higher V_{oc}. This is also supported by the reduction of the non-radiative recombination loss.[33,54,59] Wang *et al.* employed water molecules to catalyze the reaction of MAI and PbI_2 after spin-coating in SSD.[54] The V_{oc} was 13.6% higher than that of thermal annealing processed PSCs, referring to higher crystallinity and less boundaries. However, Clegg *et al.* attributed the loss of open circuit voltage to the crack and pinholes after adding water to the PbI_2 DMF.[42]

Nonradiative recombination traps contribute to the FF value as well. Larger crystal grains[39,40,48] and domains[35] caused by H_2O reduce the chances that excited carriers get trapped. For instance, Wu *et al.* added 2 wt% H_2O into the PbI_2 DMF precursor solution and hence gained a high FF of 0.85.[39] The grain size significantly increased from 50–500 nm to 500–1000 nm, equal to the thickness of the film. Also, the incorporation of water is reported to enhance the surface coverage, reducing voids and pinholes significantly when annealing in ~35% R.H.[57] However, it is not always true that the presence of H_2O has a positive effect. When Coning and coworkers increased the water content in $CH_3NH_3PbI_{3-x}Cl_x$ precursor solution, larger pinholes were observed in SEM. They likely provided direct contact between TiO_2 and P3HT, responsible for decreasing the fill factor to 0.67.[36]

The PSC device stability under humidity can also be evaluated by modeling the change of performance parameters with time[145,146] or relative humidity.[147] Darvishzadeh *et al.* modeled the change of V_{oc} with time, showing that the ion migration and PbI_2 defects are the major reasons for degradation of V_{oc} upon moisture exposure.[145] Sohrabpoor *et al.* developed models, which showed that the FF is mainly responsible for the PSC degradation.[146] Both concluded that the defect profile played a key role in the device instability.[145,146] Moreover, a drift-diffusion based model and a two-diode model were offered by Bhatt *et al.* to explain the variation of device optoelectronic and electronic parameters, *e.g.* the absorption coefficient and diffusion length as well as their effects on the device performance with different relative humidity levels.[147]

Besides the standard device parameters, the hysteresis of the *J–V* curve during the PSC measurement[148] was also significantly affected by water. Two kinds of causes for hysteresis have mainly been proposed: (1) ionic migration; (2) surface and interface defect state trapping or detrapping charges.[149,150] Mobile ions including MA^+,[149] I^-,[151,152] *etc.* migrate in the bulk point defects and the surface and grain boundaries as illustrated in Fig. 16.[153]

Moderate water contents in the film preparation could reduce the hysteresis. Wu *et al.* added a moderate amount of water to the PbI_2 DMF precursor, fabricating a well crystalline, smooth perovskite film without pinholes, detecting no hysteresis.[39] Similar suppression was observed by Gong *et al.* when adding water into the $MAPbI_{3-x}Cl_x$ precursors.[35] Gangishetty *et al.* found that the perovskite film prepared in almost 0% water exhibits severe hysteresis while the degree of hysteresis could substantially decrease as the humidity increases.[48] They attributed this to the reduced grain boundaries and traps.[48] In all of these cases, large crystal sizes and high quality films were observed with less boundaries and defects existing. This implies that less

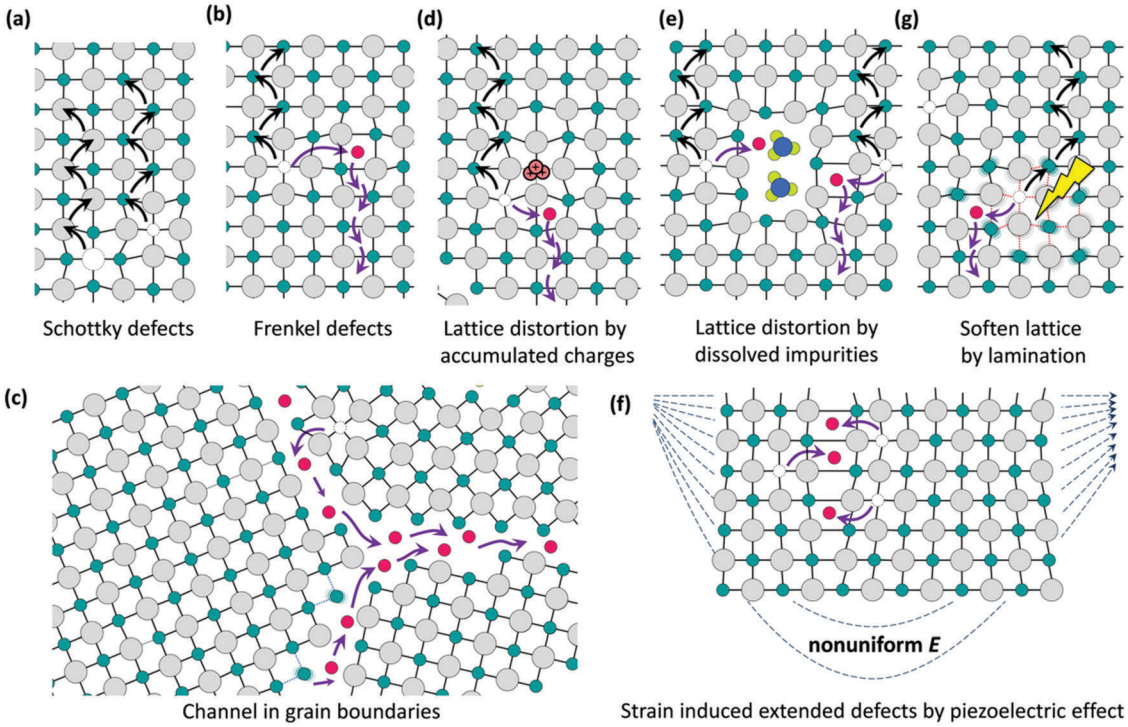

Fig. 16 Schematic diagrams illustrating the ionic migration channels. (a) Schottky defects, or vacancies; (b) Frankel defects, or interstitials defects. (c) Ion migration at the grain boundaries. Distortion of the lattice due to (d) accumulation of charges, (e) impurities, (g) light-illumination-induced lattice softening, and (f) piezoelectric effects. Reproduced from ref. 153. Copyright ©2016 American Chemical Society.

ionic channels, less defects for trapping and detrapping charges and better contact with other functional layers can be achieved.[39,48,150]

Several authors have reported that the hysteresis becomes severe when placing the PSCs under a moist atmosphere.[89,94,95] For instance, Huang *et al.* reported that the hysteresis index increased from 0.14 ± 0.06 to 0.43 ± 0.23 after 7 days of exposure.[95] While the ingressive H_2O interacts with Pb^{2+} groups to form monohydrate $MAPbI_3{\cdot}H_2O$ as well as dihydrate $MA_4PbI_6{\cdot}H_2O$, it results in lattice expansion.[94,127] Thus the bonding between MA^+ and PbI_6^{4-} becomes weak, so the activity energy for ionic migration, which is seen as the hopping process,[154] also decreases, and thereby the migration of MA^+ and I^- becomes obvious, as supported by the observations of fast degradation under an applied electronic field with moisture.[155] Therefore, increasing ionic migration leads to a severe hysteresis after H_2O ingression.

In addition to promoting migrations of ions, the moisture may induce exacerbation of hysteresis *via* increasing the amount of surface states at the surfaces and interfaces.[95,156] In the previous section, we have mentioned that the ingression of H_2O molecules destroys a whole perovskite grain into small parts and increases the number of grain boundaries. Therefore, more defect states in the surfaces and interfaces can be expected. Snaith *et al.* have proposed that the defects trap and detrap charges,[148] which is consistent with the observations in experiments.[101,157] Moreover, experiments used KPFM and AFM to prove that the grain boundaries pave the way for the motion of ions such as FA^+, and MA^+, acting like a fast transporting channel,[158] and ultimately aggravating hysteresis.[156]

To further understand the PSC stability under moisture, we summarize the performance degradation of several representative PSCs in terms of PCE in Table 3. Regardless of perovskite compositions and device architectures, PSCs undergo degradation under a humid atmosphere. However, it is still hard to make a conclusion about which kind of PSC obtains longer lifetime under exposure to H_2O since substrates, environmental factors, *etc.* all contribute to the lifetime of PSCs.

6. Recent strategies to enhance stability

Given the degradation mechanism of perovskite materials and PSCs under water, the resistance of perovskite materials to water is relevant to intrinsic perovskite characteristics and the extrinsic factors including active functional layers, and device structure. To address the issues of aquatic erosion and to sustain the longevity of the perovskite, three basic principles could be considered. Firstly, the key intrinsic improvement is to enhance the quality and stability of perovskite single crystals and perovskite films. Secondly, to avoid decay of performance, the ingression of water molecules into the perovskite needs to be inhibited or prohibited. Thirdly, to guarantee recycling of water-damaged perovskite layers, healing strategies for the cell need to be developed.

Table 3 Summary of the performance degradation of several representative PSCs under moisture exposure

No.	Test conditions	Stability	Device configuration	Ref.
1	R.H.[a] 90% (0%)[b], in the darkness, unencapsulated	3 d, 0% (~100%)[b] PCE remained	FTO/c-TiO_2[c]/meso-TiO_2[d]/$MAPbI_3$/Spiro-OMeTAD/Au	89
2	R.H. ~ 40%, at R.T.	14 d, 93% PCE remained	FTO/c-TiO_2/meso-TiO_2/$MAPbI_{3-x}Br_x$/Spiro-OMeTAD/Ag	161
3	R.H. 30–50%, 25 °C, unencapsulated	5 d, 0% PCE remained	ITO/PEDOT:PSS/$MAPbI_3$/$PC_{61}BM$/Al	141
4	R.H. 20%, ambient air, in the darkness, unencapsulated	14 d, 39% PCE remained	ITO/PEDOT:PSS/$MAPbI_3$/$PC_{61}BM$/bis-C_{60}/Ag	210
5	Under ambient conditions	275 min, 0% PCE remained	ITO/PEDOT:PSS/$MAPbI_{3-x}Cl_x$/$PC_{61}BM$/Ag	254
6	R.H. < 40%, continuous white light illumination (100 mW cm^{-2}) unencapsulated	30 min, 19% PCE remained	FTO/c-TiO_2/meso-TiO_2/$FAPbI_3$/Spiro-OMeTAD/Ag	169
7	R.H. < 40%, continuous white light illumination (100 mW cm^{-2}) unencapsulated	30 min, 33% PCE remained	FTO/c-TiO_2/meso-TiO_2/$FA_{0.9}Cs_{0.1}PbI_3$/Spiro-OMeTAD/Ag	169
8	R.H. 60% + 35 °C + under sunlight, unencapsulated	18 h, 20% PCE remained	FTO/c-TiO_2/meso-TiO_2/$MAPbI_3$/Spiro-OMeTAD/Au	11
9	R.H. 24 ± 2% + $h\nu$ (0.25–0.5 mW cm^{-2}) + 25 ± 1 °C	7 d, ~16% PCE remained	FTO/c-TiO_2/meso-TiO_2/$MAPbI_3$/Spiro-OMeTAD/Au	95

[a] R.H.: relative humidity. [b] Exposure to N_2 atmosphere. [c] c-TiO_2: compact TiO_2 layer. [d] Meso-TiO_2: mesoporous TiO_2 layer.

6.1 Stability enhancement of perovskite crystals and films in H_2O

As discussed above, the ingression of water molecules starts from the grain defects and then diffuses into the inner structure through the boundaries. The hydrogen bonds between stagnated H_2O and perovskite units release I atoms from the adjacent Pb^{2+}, which in turn react with the loose MA^+. DFT shows that the energy of $MAPbI_3$ is 0.1 eV lower than the total energy of free MAI and PbI_2 phases, indicating that a slight disturbance from water molecules could induce the decomposition of $MAPbI_3$ units.[159] Thus, improving the resistance is linked to the decrease of potential infiltration sites and the strengthening of structural bonding.[122,160]

6.1.1 Modification of perovskite components. The tenability of $RAPbX_3$ perovskite guarantees multiple ions of RA and X to improve the stability of perovskite units. Anion X, referring to I^- generally, has been partially replaced by Br^- or Cl^-, due to the stronger bonding and shorter perovskite bond length.[5,18,160–162] Besides mixed halide anions, the SCN^- anion is appealing to many researchers due to its large formation constant with Pb^{2+},[163] and $RAPbI_{3-x}SCN_x$ (RA = MA^+ or FA^+) films show less defects, better crystallinity and pronounced resistance towards moisture infiltration.[163–165] Furthermore, SCN^- additive in $FAPbI_3$ has been proven to inhibit the formation of the δ-$FAPbI_3$ phase as well as facilitate the growth of the stable α phase which eventually offers SCN^--doped $FAPbI_3$ PSCs better moisture stability.[165,166] Satyawan *et al.* proposed another latent anion BF_4^- that could partially substitute I^- to fabricate $MAPbI_{3-x}(BF_4)_x$ with similar ionic radius,[167] and lately $MAPbI_{3-x}(BF_4)_x$ has been employed in a HTL-free cell architecture by Chen and coworkers, presenting improved stability due to the hydrophobic F atom.[168]

Completely or partially using inorganic cations *e.g.* Cs^+,[169–172] 2D organic cations like small-molecule bulky ammoniums (*e.g.* $C_6H_5(CH_2)_2NH_2^+$,[173–175] $CH_3(CH_2)_3NH_3^+$,[176,177] ethylenediamine[178]) and polymer cations (*e.g.* PEI[179,180]) for the A site are of interest. 2D organic cations equip perovskite films with high stability under H_2O because of the van der Waals force in the perovskite layers making the structure robust and the hydrophobicity of 2D organic cations.[173,174,176] Nevertheless, 2D organic cations have been known for a long time to endanger the efficiency of PSCs due to the inhibition of the organic component on the carrier transport, which may hinder the passion to explore the potential of 2D or even lower dimensional organic cations.[176,181,182] Luckily a very recent study showed that the ebb of the efficiency could be mitigated by pre-heating the substrate while maintaining the resistance towards moisture.[183] Fig. 17 shows that $(BA)_2(MA)_3Pb_4I_{13}$ (BA = butylamine) exhibits a close single-crystalline quality with the inorganic perovskite component vertical to the substrate.[183] This significantly improves the carrier mobility and reduces the recombination of free charge carriers, bringing the efficiency up to 12.52% with no hysteresis and even no decrease in efficiency after encapsulation for >2000 h.

6.1.2 Fabrication of high-quality perovskite films. Polycrystalline perovskite is the primary form for perovskite studies in the optoelectronic and photovoltaic fields. Nevertheless, a general polycrystalline film consists of many small grains, accompanied by grain boundaries and interfacial defects as we discussed above. All of these play impellent roles in the penetration of H_2O. Accordingly, to improve the device stability while maintaining high efficiency, an essential demand is to synthesize a perfect polycrystalline film without remnant trapped hydrophilic molecules. In addition to carefully controlling the relative humidity at its optimal value and the exposure time in each fabrication step, studies try to adjust other process parameters and conditions of solution-based or vapor-based techniques.[29,72,184–196] Besides, traditional ceramic or polymeric membrane fabrication techniques like screen printing,[197] bar coating,[198] *etc.*,[60] are employed in PSCs.

Monocrystalline perovskites have attracted lots of interest because of their pronounced electronic properties and their role in mechanisms studies.[199,200] The impeccable crystallinity and stability ensure that perovskite single crystals are a remarkable candidate for photovoltaics.[201] This has been confirmed *via* a device structure of ITO/monocrystalline $MAPbBr_3$/Au showing stable output in moist air after exposure towards R.H. 55% for over 48 h, while that of a polycrystalline $MAPbBr_3$ based structure drops to ~60% of its initial level.[202] However, the best reported efficiency for a monocrystalline perovskite photovoltaic device is about 6%, still far below that of the certificated

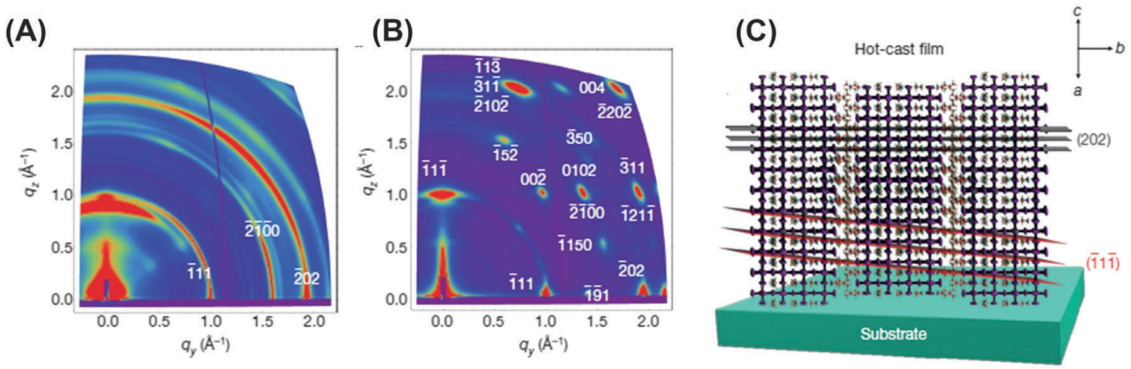

Fig. 17 (A) GIWAXS maps for room-temperature-cast polycrystalline films, and (B) hot-cast polycrystalline films. Color scale is proportional to X-ray scattering intensity. (C) Schematic representation of the (101) orientation, along with the (111) and (202) planes of a 2D perovskite crystal. Reproduced with permission from ref. 183, Copyright 2016, Nature Publishing Group.

polycrystalline PSC performance (>22%). Further research efforts such as optimizing single crystal surface properties[203] and controlling crystal facet orientation[204] are suggested to improve the monocrystalline PSC performance.

In addition, considering that $MAPbI_3$ is fabricated in working devices, the impact of interfaces and substrates can offer another effective route for enhancing the intrinsic stability of perovskite bulk films.[205,206] Recently, F4TCNQ acted as an interfacial layer in Spiro-OMeTAD/perovskite, reduced the trap states of modified perovskite by surface passivation and interfacial doping and hence improved the long-term stability.[206]

6.2 Protection of perovskite from ingression of H_2O

Although modification of the perovskite itself has a striking feature in the improvement of resistance towards moisture, most of the stability tests are still far from satisfying the standard moisture endurance requirements. To further improve the moisture tolerance, a number of studies have focused on isolating perovskite from H_2O from the view of solar cell architectures. Here, we start from the FFL to the electrode based on the device structure, and conclude with how the functional layers and device structure present their features in retarding and prohibiting the invasion of H_2O.

6.2.1 Optimization of the FFL. As we mentioned above, one of the penetration pathways for moisture is migration through the interface between $MAPbI_3$ and the FFL, including ZnO_2, TiO_2, PEDOT:PSS *etc* (Fig. 14).[207] The hydroxyl groups on the surface of ZnO in n–i–p cells and the hydrophilic and acidic properties of the hole transport layer PEDOT:PSS as the FFL in inverted p–i–n cells both accelerate the decomposition of $CH_3NH_3PbI_3$ from the contact interface. Thus, a better FFL and its interfaces with halide perovskite are required. One strategy is to further optimize the chemical properties of TiO_2, ZnO and PEDOT:PSS.[208–210] It is also noted that some studies have attempted to insert a layer into the interface, aiming to separate the perovskite from ZnO.[211–213] However, very few studies are realized *via* these optimization approaches. Instead, studies are more inclined to design new materials, classified as metal-based,[214–216] metal oxide-based[217–219] and carbon-based ones,[220–222] featuring hydrophobicity, non-corrosion and a superior contact with the organic–inorganic hybrid halide perovskite.

6.2.2 Hydrophobic treatment of perovskite films. In addition to enhancing the perovskite intrinsic stability in the presence of water as we concluded in the above section, a few studies have tried to modify the perovskite film with hydrophobic treatments. Small molecules or ionic molecules with hydrophobic groups are utilized to cover the perovskite surface, as in-site water-repulsed layers.[191,223–228] For instance, Yang and colleagues demonstrated the direct synthesis of a hydrophobic anion layer like tetraethyl ammonium (TEA) onto the perovskite film by dipping the as-formed $MAPbI_3$ film in isopropanol solution.[226] The TEA anion layer hardly impacts the efficiency compared with the control group, and it also maintained the majority of the original efficiency after storage in ~55% R.H. for 500 h.[226] Furthermore, an unprecedented concept of a "polymer/perovskite composite" was proposed in 2014,[229] featuring the isolation effect on H_2O molecules and the reduction of grain boundaries.[84,230–235] One typical example is that Zhao *et al.* introduced a PEG 3D network into the perovskite films.[231] Strikingly, PEG absorbs water molecules and stops them from reaching the perovskite grains. Further work replaced PEG with a PCBM/PEG composite to better suppress hysteresis.[233]

6.2.3 Optimization of the SFL. Spiro-OMeTAD as a SFL in an n–i–p device structure presents unsatisfactory film-forming qualities and often hydroscopic additives like Li-TFSI are employed, which go against the desire for long-term running under the operating conditions. Therefore, to alleviate the damage from water to some extent, efforts have been devoted to optimizing Spiro-OMeTAD hole transporting materials by fabricating high-quality films[236] and creating new dopants.[237–241] Another approach involving the removal of Spiro-OMeTAD is to design waterproof materials.[242–248] One of the prominent examples of designing new materials was that Zhang and coworkers applied an inorganic material $CuGaO_2$ as the HTL in the n–i–p device architecture, yielding over 18% efficiency which is comparable to that with Spiro-OMeTAD.[244] At the same time, the $CuGaO_2$-based device almost retained its high performance after 30 d of exposure to moisture (R.H. = 30–55%) while the PCE of the Spiro-OMeTAD based device went down to 3% after a week.

For the p–i–n type PSCs, the SFL is generally the electron transporting material $PC_{61}BM$. However, $PC_{61}BM$ was shown to

interact with water and easily provided pathways for the direct contact of the Al or Ag electrode with the perovskite film, all of which damages the stability of p–i–n PSCs.[141] Some studies tried to solve this problem by doping $PC_{61}BM$.[249,250] Another pathway is to employ other kinds of materials as the ETL in p–i–n type devices, like inorganic metal oxides,[141,251,252] or other organic mateirals.[250,253,254]

The longevity of PSCs could be further improved by an appropriate choice of interfacial layers.[11,252,255–262] Organic or inorganic interfacial layers lying in the electrode/SFL interface or in the SFL/perovskite interface, modified the moisture-sensitive interfaces and protected perovskite films from moisture infiltration and the degraded electrode. For instance, Niu *et al.* inserted an inert Al_2O_3 layer into the interface between Spiro-OMeTAD and $MAPbI_3$, enabling PSCs to better resist moisture at room temperature while retarding the recombination of the charges at the interface.[11]

6.2.4 Optimization of electrodes. One primary pathway for moisture infiltration is going through the electrode, and the SFL and then penetrating the inner structure of the PSCs, thus the electrode works as a forerunner to stop H_2O molecules. Two common electrode materials, Ag and Al, although low cost and possess good electron transport ability, have a poor chemical stability, not suitable for long-term operation.[143,263] A noble metal electrode Au, has shown better moisture resistance, but the high cost limits it in the large-area fabrication and a recent study reported that it could trap water molecules[144] and was able to diffuse through the hole transporting layer.[264] More recently, Huang *et al.* presented the very appealing potential of Cu electrodes in PSCs.[265,266] The unencapsulated PSCs employing Cu electrodes could maintain almost 100% of the original efficiency value after being placed in ~55% R.H. at room temperature for over 800 hours.[266] However, Cu metal undergoes oxidation to $Cu(OH)_2$ and/or CuO_x after exposure to oxygen or moisture, and thus it still requires strict encapsulation for practical applications. To date, a widely-accepted hydrophobic material is the carbon family including graphite, carbon black, mesoporous carbon and some graphene-derived nanomaterials.[267] This family not only provides chemical stability, substantially increasing the hydrophobicity of PSCs, but also maintains good conductivity with low cost. Han *et al.* successfully developed a typical model based on a triple-layer structure $TiO_2/ZrO_2/MAPbI_3$ with 5-AVA additive.[197] The unchanged output in 1000 h is ascribed to the stable contact of TiO_2 with perovskite and the hydrophilic effect of the porous carbon electrode which blocks upper moisture completely.[197,207] Further studies improved its efficiency up to 15%, making it more competitive compared with the highly performing metal electrode-based PSCs.[268]

6.2.5 Device encapsulation. Given the success of the device encapsulation technique in organic light emitting diodes, dye-sensitizer solar cells and polymer solar cells, it has also been applied in PSCs to isolate H_2O chemically at the molecular level or to block H_2O mechanically at the macroscopic level. Encapsulation has shown its simplicity by only spinning casting and drying the hydrophobic polymer Teflon on top of the electrode while maintaining superior hydrophobicity towards moisture.[269] Encapsulation stability also demonstrated its viability *via* outdoor tests operated, respectively, in Jeddah, Saudi Arabia[270] and Hong Kong.[271] These all indicated the plausible tolerance of encapsulation in PSCs towards natural environmental conditions. However, moisture still slowly penetrates inside through the edges of the adhesive layer or directly through the sealing material (Fig. 18),[272–274] showing immeasurable damage capacity especially at 85 °C.[272] The still limited longevity of encapsulated PSCs points out that the choice of sealing materials and the airtightness of the contact interfaces between the encapsulated materials require more attention in the future. Furthermore, Wilderspin *et al.*, for the first time, proposed a very simple approach based on RGB analysis to evaluate the feasibility and effectiveness of encapsulation approaches.[275] However, to meet the demand of finding a more robust sealing method and evaluation of other techniques for improved stability, we believe that more feasible and highly effective assessment methods should be developed in the future.

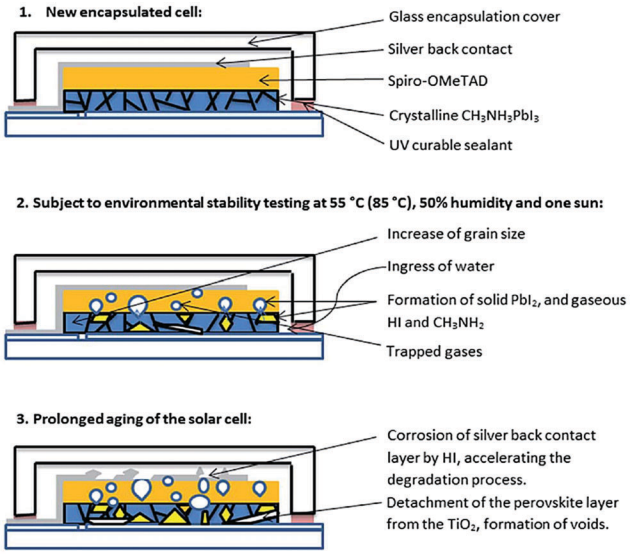

Fig. 18 Scheme of the degradation processes of encapsulated methylammonium lead iodide perovskite solar cells illuminated at elevated temperatures and high humidity. Reproduced from ref. 274, with permission from The Royal Society of Chemistry.

6.3 Curing decomposed perovskite caused by H_2O

Although much work has been done to improve the stability of perovskite films and the corresponding devices which we also emphasized above, the existence of damaged perovskite films seems to be inevitable during device preparation and utility, indicating the importance of healing lacerated perovskite films. Now, a few curing approaches have been discovered and adapted to recover the original performance,[100,231,276–279] and some are especially for water-induced deterioration, presenting promising healing effects.[90,231,276] Zhao *et al.* have demonstrated that no loss of MAI played a key role in voluntary, complete reformation of $CH_3NH_3PbI_3$ powders after drying water.[90] In PSCs, a 3D polymer scaffold PEG was applied to provide the $CH_3NH_3PbI_3$ film with self-healing abilities.[231]

The recovered films exhibit compatible output compared with the initial performance, while the light absorption and J_{sc} get improved after this recovery. In addition, the recovery can also be realized by other approaches like light irradiation, low moisture exposure, and thermal annealing.[276] By providing extra energy, respectively, they could drive complete recovery from decomposed phases to the tetragonal perovskite phase in several hours, offering effective and feasible routes to retreive the spoiled goods in large-scale industrial production as well as sustain the working devices in outdoor environments. It is demonstrated that both LiTFSI and TBP cause the Spiro-OMeTAD layer to be fragile upon thermal annealing and light irradiation.[280–283] Therefore, these two healing strategies should be avoided with sensitive materials. In fact, considering that the PSCs suffer from thermal stress and irradiation during long-term operation, further development of other stable Spiro-OMeTAD additives or stable hole transporting materials is one of the critical issues for operation in a natural environment.

7. Conclusions and outlook

In this review, we have analyzed the main impacts of water in various stages of the lifecycle of the state-of-the-art lead-based PSCs. It was shown that moderate water amounts could facilitate the nucleation and crystallization of the perovskite, resulting in better perovskite film quality and increased PSC performance. However, water irreversibly destroys the perovskite materials after reaching a certain level, but they exhibit better tolerance against water than initially expected. Hence, humidity resistant fabrication of high-performance PSC devices and modules is required. Generally, water shows a negative effect on the long-term stability of PSCs. Self-healing behavior has been found in perovskite materials and the recovery of PSC performance can be realized by adopting appropriate measures.

Research on elucidating the connection of perovskite materials and solar cells with H_2O has made significant progress in the past few years. Nevertheless, there are still some basic questions and practical issues regarding this connection in the fabrication process and long-term operation, which require further considerations elaborated in the following. Protection methods should be adopted to reduce the water effect during the practical operation of a PSC.

7.1 Materials and device structure

The role of water in the fabrication part is often related to $MAPbI_3$, but more knowledge on other doped perovskites is likewise needed, because recent high-performance PSCs contain Cl^-/Br^- or are doped with FA^+. The controversies found in the literature indicate that the impact of water could also be attributed to other factors, *e.g.* device structures, which calls for a more systematic study of the affecting factors. To meet the trend of green solar cells, less-lead or lead-free perovskite materials should be developed. The present development work on lead-free perovskite materials such as Sn, Bi, Cu, and Sb based perovskites and derivatives as well as double perovskites often focus on intrinsic properties and optoelectronic performance, whereas their relationship to water is not adequately addressed. Hence, it would be beneficial to provide a reference value for water tolerance for practical cases.

7.2 Fabrication

Previous studies have mainly dealt with the impact of water in single fabrication steps, which enhance the understanding of the influence of H_2O. However, studies which consider water or moisture in the whole synthetic process are very few. Better understanding of the acceptable range or steady optimized value of water amount in the whole process could help to reduce the complexity of the fabrication. In spin-coating processes, which are often bound to small-scale applications, the influences of water are well-known, whereas in the case of scalable industrial production such as screen printing, more research on the impact of water is still required. Concerning real applications of PSCs, the fabrication technique is of upmost importance to costs and volume meaning that identifying first the fabrication method could be useful followed by optimization of control of water in each stage, which may also necessitate lab studies.

A literature study showed that an appropriate amount of water in perovskite raw ingredients or precursor solutions has a positive effect, which suggests that water as an additive could improve the quality of perovskites. In the later fabrication steps, water mainly appears in the form of moisture during the film growth requiring precise control of the relative humidity. One feasible strategy to ensure correct the humidity ratio could be to use a gas mixture of water vapor and dry air in a given ratio and at thermal equilibrium, *i.e.* at the same temperature. When the humidity is difficult to control in the fabrication, an alternative pathway would be to develop water resistant fabrication methods based on compositionally modified or doped perovskites, or to use water absorbents which protect perovskite growth from moisture. The behavior of PSC modules under real conditions against H_2O is not yet clear. The synergistic effect of H_2O, light, and thermal stress on module size deserves more research in the near future.

7.3 Stability

Despite recent progress, the full basic understanding of the stability of the perovskite layer and its interfaces against moisture is still far from complete. For example, confirmation of gaseous decomposition products may require the use of isotope tracer techniques. The role of the interface in the moisture ingression is also unclear.

As the decomposition of perovskite films and devices seems to accelerate only after a certain amount of water, stability could be increased by improving the intrinsic perovskite film and optimizing device architectures. Furthermore, one could also expect that entirely eliminating H_2O in the encapsulating step and improving the encapsulation techniques could enhance long-term operation in natural environments. This would also require stricter stability screening and considering the combined effects of water with other environmental factors when evaluating a new material or encapsulation technique. Following closer established

procedures for environmental testing such as ISOS, IEC (61646), and long-term outdoor tests would be beneficial in this context. For PSC one could also consider introducing water vapor transmission rate (WVTR) and oxygen transmission rate (OTR) as additional test variables to be monitored, which are encapsulation quality concepts often used in organic light-emitting diodes and organic polymer solar cells.

Conflicts of interest

There are no conflicts to declare.

Acknowledgements

We would like to acknowledge the financial support from the National Natural Science Foundation of China (NSFC) grant 21576218, the funding from the State Key Laboratory of Multiphase Flow in Power Engineering and the Administrative Department for Undergraduate Education, Xi'an Jiaotong University. Peter D. Lund acknowledges the financial support from Academy of Finland (Grant No. 13282962 and 13279204). Huanping Zhou acknowledges the financial support from the NSFC grant 51672008.

References

1 A. Kojima, K. Teshima, Y. Shirai and T. Miyasaka, *J. Am. Chem. Soc.*, 2009, **131**, 6050–6051.
2 National Renewable Energy Laboratory, http://www.nrel.gov/pv/assets/images/efficiency_chart.jpg, accessed December, 2016.
3 C. D. Bailie, M. G. Christoforo, J. P. Mailoa, A. R. Bowring, E. L. Unger, W. H. Nguyen, J. Burschka, N. Pellet, J. Z. Lee, M. Gratzel, R. Noufi, T. Buonassisi, A. Salleo and M. D. McGehee, *Energy Environ. Sci.*, 2015, **8**, 956–963.
4 G. Xing, N. Mathews, S. S. Lim, N. Yantara, X. Liu, D. Sabba, M. Grätzel, S. Mhaisalkar and T. C. Sum, *Nat. Mater.*, 2014, **13**, 476–480.
5 J. H. Noh, S. H. Im, J. H. Heo, T. N. Mandal and S. I. Seok, *Nano Lett.*, 2013, **13**, 1764–1769.
6 H. J. Snaith, *J. Phys. Chem. Lett.*, 2013, **4**, 3623–3630.
7 T.-B. Song, Q. Chen, H. Zhou, C. Jiang, H.-H. Wang, Y. Yang, Y. Liu, J. You and Y. Yang, *J. Mater. Chem. A*, 2015, **3**, 9032–9050.
8 N. S. Lewis, *Science*, 2016, **351**, aad1920.
9 A. Polman, M. Knight, E. C. Garnett, B. Ehrler and W. C. Sinke, *Science*, 2016, **352**, aad4424.
10 T. Leijtens, G. E. Eperon, N. K. Noel, S. N. Habisreutinger, A. Petrozza and H. J. Snaith, *Adv. Energy Mater.*, 2015, **5**, 1500963.
11 G. Niu, W. Li, F. Meng, L. Wang, H. Dong and Y. Qiu, *J. Mater. Chem. A*, 2014, **2**, 705–710.
12 T. M. Koh, K. Thirumal, H. S. Soo and N. Mathews, *ChemSusChem*, 2016, **9**, 2541–2558.
13 H. Zhou, Q. Chen, G. Li, S. Luo, T.-B. Song, H.-S. Duan, Z. Hong, J. You, Y. Liu and Y. Yang, *Science*, 2014, **345**, 542–546.
14 J. Burschka, N. Pellet, S.-J. Moon, R. Humphry-Baker, P. Gao, M. K. Nazeeruddin and M. Gratzel, *Nature*, 2013, **499**, 316–319.
15 M. Liu, M. B. Johnston and H. J. Snaith, *Nature*, 2013, **501**, 395–398.
16 Q. Chen, H. Zhou, Z. Hong, S. Luo, H.-S. Duan, H.-H. Wang, Y. Liu, G. Li and Y. Yang, *J. Am. Chem. Soc.*, 2014, **136**, 622–625.
17 P. Gao, M. Gratzel and M. K. Nazeeruddin, *Energy Environ. Sci.*, 2014, **7**, 2448–2463.
18 M. M. Lee, J. Teuscher, T. Miyasaka, T. N. Murakami and H. J. Snaith, *Science*, 2012, **338**, 643–647.
19 C.-Y. Chang, Y.-C. Huang, C.-S. Tsao and W.-F. Su, *ACS Appl. Mater. Interfaces*, 2016, **8**, 26712–26721.
20 M. Anaya, J. F. Galisteo-Lopez, M. E. Calvo, C. Lopez and H. Miguez, *J. Phys. Chem. C*, 2016, **120**, 3071–3076.
21 Y. C. Zheng, S. Yang, X. Chen, Y. Chen, Y. Hou and H. G. Yang, *Chem. Mater.*, 2015, **27**, 5116–5121.
22 Y. Fu, F. Meng, M. B. Rowley, B. J. Thompson, M. J. Shearer, D. Ma, R. J. Hamers, J. C. Wright and S. Jin, *J. Am. Chem. Soc.*, 2015, **137**, 5810–5818.
23 S. Yang, Y. C. Zheng, Y. Hou, X. Chen, Y. Chen, Y. Wang, H. Zhao and H. G. Yang, *Chem. Mater.*, 2014, **26**, 6705–6710.
24 C.-W. Chen, H.-W. Kang, S.-Y. Hsiao, P.-F. Yang, K.-M. Chiang and H.-W. Lin, *Adv. Mater.*, 2014, **26**, 6647–6652.
25 M. M. Tavakoli, L. Gu, Y. Gao, C. Reckmeier, J. He, A. L. Rogach, Y. Yao and Z. Fan, *Sci. Rep.*, 2015, **5**, 14083.
26 P. Pistor, J. Borchert, W. Fraenzel, R. Csuk and R. Scheer, *J. Phys. Chem. Lett.*, 2014, **5**, 3308–3312.
27 J. Borchert, H. Boht, W. Fraenzel, R. Csuk, R. Scheer and P. Pistor, *J. Mater. Chem. A*, 2015, **3**, 19842–19849.
28 M. R. Leyden, L. K. Ono, S. R. Raga, Y. Kato, S. Wang and Y. Qi, *J. Mater. Chem. A*, 2014, **2**, 18742–18745.
29 P. Luo, Z. Liu, W. Xia, C. Yuan, J. Cheng and Y. Lu, *ACS Appl. Mater. Interfaces*, 2015, **7**, 2708–2714.
30 B. Yang, J. Keum, O. S. Ovchinnikova, A. Belianinov, S. Chen, M.-H. Du, I. N. Ivanov, C. M. Rouleau, D. B. Geohegan and K. Xiao, *J. Am. Chem. Soc.*, 2016, **138**, 5028–5035.
31 G. E. Eperon, S. N. Habisreutinger, T. Leijtens, B. J. Bruijnaers, J. J. van Franeker, D. W. deQuilettes, S. Pathak, R. J. Sutton, G. Grancini, D. S. Ginger, R. A. J. Janssen, A. Petrozza and H. J. Snaith, *ACS Nano*, 2015, **9**, 9380–9393.
32 J. Schoonman, *Chem. Phys. Lett.*, 2015, **619**, 193–195.
33 L. Ling, S. Yuan, P. Wang, H. Zhang, L. Tu, J. Wang, Y. Zhan and L. Zheng, *Adv. Funct. Mater.*, 2016, **26**, 5028–5034.
34 Z. Wang, S. Yuan, D. Li, F. Jin, R. Zhang, Y. Zhan, M. Lu, S. Wang, Y. Zheng, J. Guo, Z. Fan and L. Chen, *Opt. Express*, 2016, **24**, A1431–A1443.
35 X. Gong, M. Li, X.-B. Shi, H. Ma, Z.-K. Wang and L.-S. Liao, *Adv. Funct. Mater.*, 2015, **25**, 6671–6678.
36 B. Conings, A. Babayigit, T. Vangerven, J. D'Haen, J. Manca and H.-G. Boyen, *J. Mater. Chem. A*, 2015, **3**, 19123–19128.
37 C. Aranda, C. Cristobal, L. Shooshtari, C. Li, S. Huettner and A. Guerrero, *Sustain. Energy Fuels*, 2017, **1**, 540–547.

38 S. Rahimnejad, A. Kovalenko, S. M. Fores, C. Aranda and A. Guerrero, *ChemPhysChem*, 2016, **17**, 2795–2798.
39 C.-G. Wu, C.-H. Chiang, Z.-L. Tseng, M. K. Nazeeruddin, A. Hagfeldt and M. Grätzel, *Energy Environ. Sci.*, 2015, **8**, 2725–2733.
40 N. Adhikari, A. Dubey, E. A. Gaml, B. Vaagensmith, K. M. Reza, S. A. A. Mabrouk, S. Gu, J. Zai, X. Qian and Q. Qiao, *Nanoscale*, 2016, **8**, 2693–2703.
41 T. Miyadera, Y. Shibata, T. Koganezawa, T. N. Murakami, T. Sugita, N. Tanigaki and M. Chikamatsu, *Nano Lett.*, 2015, **15**, 5630–5634.
42 C. Clegg and I. G. Hill, *RSC Adv.*, 2016, **6**, 52448–52458.
43 H. Gao, C. Bao, F. Li, T. Yu, J. Yang, W. Zhu, X. Zhou, G. Fu and Z. Zou, *ACS Appl. Mater. Interfaces*, 2015, **7**, 9110–9117.
44 Z. Huang, X. Duan, Y. Zhang, X. Hu, L. Tan and Y. Chen, *Sol. Energy Mater. Sol. Cells*, 2016, **155**, 166–175.
45 Q. Liang, J. Liu, Z. Cheng, Y. Li, L. Chen, R. Zhang, J. Zhang and Y. Han, *J. Mater. Chem. A*, 2016, **4**, 223–232.
46 J. Kim, J. S. Yun, X. Wen, A. M. Soufiani, C. F. J. Lau, B. Wilkinson, J. Seidel, M. A. Green, S. Huang and A. W. Y. Ho-Baillie, *J. Phys. Chem. C*, 2016, **120**, 11262–11267.
47 Y. H. Lee, J. Luo, R. Humphry-Baker, P. Gao, M. Grätzel and M. K. Nazeeruddin, *Adv. Funct. Mater.*, 2015, **25**, 3925–3933.
48 M. K. Gangishetty, R. W. J. Scott and T. L. Kelly, *Nanoscale*, 2016, **8**, 6300–6307.
49 Y. Xu, L. Zhu, J. Shi, X. Xu, J. Xiao, J. Dong, H. Wu, Y. Luo, D. Li and Q. Meng, *ChemPhysChem*, 2016, **17**, 112–118.
50 B. Yang, O. Dyck, J. Poplawsky, J. Keum, S. Das, A. Puretzky, T. Aytug, P. C. Joshi, C. M. Rouleau, G. Duscher, D. B. Geohegan and K. Xiao, *Angew. Chem., Int. Ed.*, 2015, **54**, 14862–14865.
51 R. Lindblad, D. Bi, B. W. Park, J. Oscarsson, M. Gorgoi, H. Siegbahn, M. Odelius, E. M. Johansson and H. Rensmo, *J. Phys. Chem. Lett.*, 2014, **5**, 648–653.
52 B. Jeong, S. M. Cho, S. H. Cho, J. H. Lee, I. Hwang, S. K. Hwang, J. Cho, T.-W. Lee and C. Park, *Phys. Status Solidi RRL*, 2016, **10**, 381–387.
53 P. Fedeli, F. Gazza, D. Calestani, P. Ferro, T. Besagni, A. Zappettini, G. Calestani, E. Marchi, P. Ceroni and R. Mosca, *J. Phys. Chem. C*, 2015, **119**, 21304–21313.
54 B. Wang, Z.-G. Zhang, S. Ye, H. Rao, Z. Bian, C. Huang and Y. Li, *J. Mater. Chem. A*, 2016, **4**, 17267–17273.
55 J. Huang, X. Yu, J. Xie, D. Xu, Z. Tang, C. Cui and D. Yang, *ACS Appl. Mater. Interfaces*, 2016, **8**, 21505–21511.
56 J. A. Aguiar, S. Wozny, N. R. Alkurd, M. Yang, L. Kovarik, T. G. Holesinger, M. Al-Jassim, K. Zhu, W. Zhou and J. J. Berry, *ACS Energy Lett.*, 2016, **1**, 155–161.
57 J. You, Y. Yang, Z. Hong, T.-B. Song, L. Meng, Y. Liu, C. Jiang, H. Zhou, W.-H. Chang, G. Li and Y. Yang, *Appl. Phys. Lett.*, 2014, **105**, 183902.
58 S. R. Raga, M.-C. Jung, M. V. Lee, M. R. Leyden, Y. Kato and Y. Qi, *Chem. Mater.*, 2015, **27**, 1597–1603.
59 S. Pathak, A. Sepe, A. Sadhanala, F. Deschler, A. Haghighirad, N. Sakai, K. C. Goedel, S. D. Stranks, N. Noel and M. Price, *ACS Nano*, 2015, **9**, 2311–2320.
60 J. H. Kim, S. T. Williams, N. Cho, C.-C. Chueh and A. K. Y. Jen, *Adv. Energy Mater.*, 2015, **5**, 1401229.
61 J. Liu, C. Gao, X. He, Q. Ye, L. Ouyang, D. Zhuang, C. Liao, J. Mei and W. Lau, *ACS Appl. Mater. Interfaces*, 2015, **7**, 24008–24015.
62 K. K. Bass, R. E. McAnally, S. Zhou, P. I. Djurovich, M. E. Thompson and B. C. Melot, *Chem. Commun.*, 2014, **50**, 15819–15822.
63 S. Berweger, G. A. MacDonald, M. Yang, K. J. Coakley, J. J. Berry, K. Zhu, F. W. DelRio, T. M. Wallis and P. Kabos, *Nano Lett.*, 2017, **17**, 1796–1801.
64 J. A. Aguiar, S. Wozny, T. G. Holesinger, T. Aoki, M. K. Patel, M. Yang, J. J. Berry, M. Al-Jassim, W. Zhou and K. Zhu, *Energy Environ. Sci.*, 2016, **9**, 2372–2382.
65 Z. Xiao, Q. Dong, C. Bi, Y. Shao, Y. Yuan and J. Huang, *Adv. Mater.*, 2014, **26**, 6503–6509.
66 Q.-Q. Ge, J. Ding, J. Liu, J.-Y. Ma, Y.-X. Chen, X.-X. Gao, L.-J. Wan and J.-S. Hu, *J. Mater. Chem. A*, 2016, **4**, 13458–13467.
67 Y. Jiang, E. J. Juarez-Perez, Q. Ge, S. Wang, M. R. Leyden, L. K. Ono, S. R. Raga, J. Hu and Y. Qi, *Mater. Horiz.*, 2016, **3**, 548–555.
68 Z. Zhou, Z. Wang, Y. Zhou, S. Pang, D. Wang, H. Xu, Z. Liu, N. P. Padture and G. Cui, *Angew. Chem., Int. Ed.*, 2015, **54**, 9705–9709.
69 S. Pang, Y. Zhou, Z. Wang, M. Yang, A. R. Krause, Z. Zhou, K. Zhu, N. P. Padture and G. Cui, *J. Am. Chem. Soc.*, 2016, **138**, 750–753.
70 W. Peng, B. Anand, L. Liu, S. Sampat, B. E. Bearden, A. V. Malko and Y. J. Chabal, *Nanoscale*, 2016, **8**, 1627–1634.
71 W. Zhou, Y. Zhao, C. Shi, H. Huang, J. Wei, R. Fu, K. Liu, D. Yu and Q. Zhao, *J. Phys. Chem. Lett.*, 2016, **120**, 4759–4765.
72 H. Zhang, J. Mao, H. He, D. Zhang, H. L. Zhu, F. Xie, K. S. Wong, M. Grätzel and W. C. H. Choy, *Adv. Energy Mater.*, 2015, **5**, 1501354.
73 F. Liu, Q. Dong, M. K. Wong, A. B. Djurišić, A. Ng, Z. Ren, Q. Shen, C. Surya, W. K. Chan, J. Wang, A. M. C. Ng, C. Liao, H. Li, K. Shih, C. Wei, H. Su and J. Dai, *Adv. Energy Mater.*, 2016, **6**, 1502206.
74 M. L. Petrus, Y. Hu, D. Moia, P. Calado, A. M. A. Leguy, P. R. F. Barnes and P. Docampo, *ChemSusChem*, 2016, **9**, 2699–2707.
75 Y. Lei, L. Gu, W. He, Z. Jia, X. Yang, H. Jia and Z. Zheng, *J. Mater. Chem. A*, 2016, **4**, 5474–5481.
76 M. Lv, X. Dong, X. Fang, B. Lin, S. Zhang, X. Xu, J. Ding and N. Yuan, *RSC Adv.*, 2015, **5**, 93957–93963.
77 S. R. Raga, L. K. Ono and Y. Qi, *J. Mater. Chem. A*, 2016, **4**, 2494–2500.
78 J. B. Patel, R. L. Milot, A. D. Wright, L. M. Herz and M. B. Johnston, *J. Phys. Chem. Lett.*, 2015, **7**, 96–102.
79 Y. Li, X. Xu, C. Wang, C. Wang, F. Xie, J. Yang and Y. Gao, *J. Phys. Chem. C*, 2015, **119**, 23996–24002.
80 R. Ruess, F. Benfer, F. Böcher, M. Stumpp and D. Schlettwein, *ChemPhysChem*, 2016, **17**, 1505–1511.
81 J. Yang, B. D. Siempelkamp, D. Liu and T. L. Kelly, *ACS Nano*, 2015, **9**, 1955–1963.
82 B. Yang, O. Dyck, W. Ming, M.-H. Du, S. Das, C. M. Rouleau, G. Duscher, D. B. Geohegan and K. Xiao, *ACS Appl. Mater. Interfaces*, 2016, **8**, 32333–32340.

83 M. Ledinsky, P. Loper, B. Niesen, J. Holovsky, S. J. Moon, J. H. Yum, S. De Wolf, A. Fejfar and C. Ballif, *J. Phys. Chem. Lett.*, 2015, **6**, 401–406.
84 N. A. Manshor, Q. Wali, K. K. Wong, S. K. Muzakir, A. Fakharuddin, L. Schmidt-Mende and R. Jose, *Phys. Chem. Chem. Phys.*, 2016, **18**, 21629–21639.
85 A. J. Pearson, G. E. Eperon, P. E. Hopkinson, S. N. Habisreutinger, J. T.-W. Wang, H. J. Snaith and N. C. Greenham, *Adv. Energy Mater.*, 2016, **6**, 1600014.
86 T. Baikie, Y. Fang, J. M. Kadro, M. Schreyer, F. Wei, S. G. Mhaisalkar, M. Graetzel and T. J. White, *J. Mater. Chem. A*, 2013, **1**, 5628–5641.
87 I. Deretzis, A. Alberti, G. Pellegrino, E. Smecca, F. Giannazzo, N. Sakai, T. Miyasaka and A. La Magna, *Appl. Phys. Lett.*, 2015, **106**, 131904.
88 A. Alberti, I. Deretzis, G. Pellegrino, C. Bongiorno, E. Smecca, G. Mannino, F. Giannazzo, G. G. Condorelli, N. Sakai, T. Miyasaka, C. Spinella and A. La Magna, *ChemPhysChem*, 2015, **16**, 3064–3071.
89 J. A. Christians, P. A. Miranda Herrera and P. V. Kamat, *J. Am. Chem. Soc.*, 2015, **137**, 1530–1538.
90 J. Zhao, B. Cai, Z. Luo, Y. Dong, Y. Zhang, H. Xu, B. Hong, Y. Yang, L. Li, W. Zhang and C. Gao, *Sci. Rep.*, 2016, **6**, 21976.
91 W. Wei and Y. H. Hu, *Int. J. Energy Res.*, 2016, **41**, 1063–1069.
92 W.-C. Lin, H.-Y. Chang, K. Abbasi, J.-J. Shyue and C. Burda, *Adv. Mater. Interfaces*, 2017, **4**, 1600673.
93 D. Li, S. A. Bretschneider, V. W. Bergmann, I. M. Hermes, J. Mars, A. Klasen, H. Lu, W. Tremel, M. Mezger, H.-J. Butt, S. A. L. Weber and R. Berger, *J. Phys. Chem. C*, 2016, **120**, 6363–6368.
94 A. M. A. Leguy, Y. Hu, M. Campoy-Quiles, M. I. Alonso, O. J. Weber, P. Azarhoosh, M. van Schilfgaarde, M. T. Weller, T. Bein, J. Nelson, P. Docampo and P. R. F. Barnes, *Chem. Mater.*, 2015, **27**, 3397–3407.
95 W. Huang, J. S. Manser, P. V. Kamat and S. Ptasinska, *Chem. Mater.*, 2015, **28**, 303–311.
96 B. Philippe, B.-W. Park, R. Lindblad, J. Oscarsson, S. Ahmadi, E. M. J. Johansson and H. Rensmo, *Chem. Mater.*, 2015, **27**, 1720–1731.
97 M. Shirayama, M. Kato, T. Miyadera, T. Sugita, T. Fujiseki, S. Hara, H. Kadowaki, D. Murata, M. Chikamatsu and H. Fujiwara, *J. Appl. Phys.*, 2016, **119**, 115501.
98 A. M. Askar, G. M. Bernard, B. Wiltshire, K. Shankar and V. K. Michaelis, *J. Phys. Chem. C*, 2017, **121**, 1013–1024.
99 W. Hao, X. Chen and S. Li, *J. Phys. Chem. C*, 2016, **120**, 28448–28455.
100 Q.-D. Dao, R. Tsuji, A. Fujii and M. Ozaki, *Org. Electron.*, 2017, **43**, 229–234.
101 N. Ahn, K. Kwak, M. S. Jang, H. Yoon, B. Y. Lee, J.-K. Lee, P. V. Pikhitsa, J. Byun and M. Choi, *Nat. Commun.*, 2016, **7**, 13422.
102 L. Zhang and P. H. L. Sit, *RSC Adv.*, 2016, **6**, 76938–76947.
103 B.-A. Chen, J.-T. Lin, N.-T. Suen, C.-W. Tsao, T.-C. Chu, Y.-Y. Hsu, T.-S. Chan, Y.-T. Chan, J.-S. Yang, C.-W. Chiu and H. M. Chen, *ACS Energy Lett.*, 2017, **2**, 342–348.
104 C. Wang, Y. Li, X. Xu, C. Wang, F. Xie and Y. Gao, *Chem. Phys. Lett.*, 2015, **649**, 151–155.
105 A. R. Milosavljević, W. Huang, S. Sadhu and S. Ptasinska, *Angew. Chem., Int. Ed.*, 2016, **55**, 10083–10087.
106 S. Sarina, E. R. Waclawik and H. Zhu, *Green Chem.*, 2013, **15**, 1814–1833.
107 R. K. Rai, D. Tyagi, K. Gupta and S. K. Singh, *Catal. Sci. Technol.*, 2016, **6**, 3341–3361.
108 J. Xiong, B. Yang, C. Cao, R. Wu, Y. Huang, J. Sun, J. Zhang, C. Liu, S. Tao, Y. Gao and J. Yang, *Org. Electron.*, 2016, **30**, 30–35.
109 L. Hu, G. Shao, T. Jiang, D. Li, X. Lv, H. Wang, X. Liu, H. Song, J. Tang and H. Liu, *ACS Appl. Mater. Interfaces*, 2015, **7**, 25113–25120.
110 E. Mosconi, J. M. Azpiroz and F. De Angelis, *Chem. Mater.*, 2015, **27**, 4885–4892.
111 Y. Liu, K. Palotas, X. Yuan, T. Hou, H. Lin, Y. Li and S.-T. Lee, *ACS Nano*, 2017, **11**, 2060–2065.
112 C.-H. Chiang and C.-G. Wu, *ChemSusChem*, 2016, **9**, 2666–2672.
113 Q. Wang, B. Chen, Y. Liu, Y. Deng, Y. Bai, Q. Dong and J. Huang, *Energy Environ. Sci.*, 2017, **10**, 516–522.
114 J. M. Frost, K. T. Butler, F. Brivio, C. H. Hendon, M. van Schilfgaarde and A. Walsh, *Nano Lett.*, 2014, **14**, 2584–2590.
115 B. Murali, S. Dey, A. L. Abdelhady, W. Peng, E. Alarousu, A. R. Kirmani, N. Cho, S. P. Sarmah, M. R. Parida, M. I. Saidaminov, A. A. Zhumekenov, J. Sun, M. S. Alias, E. Yengel, B. S. Ooi, A. Amassian, O. M. Bakr and O. F. Mohammed, *ACS Energy Lett.*, 2016, **1**, 1119–1126.
116 G. Grancini, V. D'Innocenzo, E. R. Dohner, N. Martino, A. R. Srimath Kandada, E. Mosconi, F. De Angelis, H. I. Karunadasa, E. T. Hoke and A. Petrozza, *Chem. Sci.*, 2015, **6**, 7305–7310.
117 N. Z. Koocher, D. Saldana-Greco, F. Wang, S. Liu and A. M. Rappe, *J. Phys. Chem. Lett.*, 2015, **6**, 4371–4378.
118 C.-J. Tong, W. Geng, Z.-K. Tang, C.-Y. Yam, X.-L. Fan, J. Liu, W.-M. Lau and L.-M. Liu, *J. Phys. Chem. Lett.*, 2015, **6**, 3289–3295.
119 C. Müller, T. Glaser, M. Plogmeyer, M. Sendner, S. Döring, A. A. Bakulin, C. Brzuska, R. Scheer, M. S. Pshenichnikov, W. Kowalsky, A. Pucci and R. Lovrinčić, *Chem. Mater.*, 2015, **27**, 7835–7841.
120 W. Geng, L. Zhang, Y.-N. Zhang, W.-M. Lau and L.-M. Liu, *J. Phys. Chem. C*, 2014, **118**, 19565–19571.
121 H. Xin, T. R. Paudel, P. A. Dowben, D. Shuai and E. Y. Tsymbal, *Phys. Rev. B: Condens. Matter Mater. Phys.*, 2016, **94**, 195309.
122 H. Fang and P. Jena, *J. Mater. Chem. A*, 2016, **4**, 4728–4737.
123 L. Zhang and P. H. L. Sit, *J. Phys. Chem. C*, 2015, **119**, 22370–22378.
124 J. Yang, B. D. Siempelkamp, E. Mosconi, F. De Angelis and T. L. Kelly, *Chem. Mater.*, 2015, **27**, 4229–4236.
125 Q. Lv, W. He, Z. Lian, J. Ding, Q. Li and Q. Yan, *CrystEngComm*, 2017, **19**, 901–904.
126 F. Hao, C. C. Stoumpos, Z. Liu, R. P. Chang and M. G. Kanatzidis, *J. Am. Chem. Soc.*, 2014, **136**, 16411–16419.

127 Z. Zhu, V. G. Hadjiev, Y. Rong, R. Guo, B. Cao, Z. Tang, F. Qin, Y. Li, Y. Wang, F. Hao, S. Venkatesan, W. Li, S. Baldelli, A. M. Guloy, H. Fang, Y. Hu, Y. Yao, Z. Wang and J. Bao, *Chem. Mater.*, 2016, **28**, 7385–7393.
128 A. Arakcheeva, D. Chernyshov, M. Spina, L. Forro and E. Horvath, *Acta Crystallogr., Sect. B: Struct. Sci.*, 2016, **72**, 716–722.
129 G. H. Imler, X. Li, B. Xu, G. E. Dobereiner, H. L. Dai, Y. Rao and B. B. Wayland, *Chem. Commun.*, 2015, **51**, 11290–11292.
130 C. Qin, T. Matsushima, T. Fujihara, W. J. Potscavage, Jr. and C. Adachi, *Adv. Mater.*, 2015, **28**, 466–471.
131 Z. Song, A. Abate, S. C. Watthage, G. K. Liyanage, A. B. Phillips, U. Steiner, M. Graetzel and M. J. Heben, *Adv. Energy Mater.*, 2016, **6**, 1600846.
132 R. Long, W. Fang and O. V. Prezhdo, *J. Phys. Chem. Lett.*, 2016, **7**, 3215–3222.
133 J. A. Christians, J. S. Manser and P. V. Kamat, *J. Phys. Chem. Lett.*, 2015, **6**, 2086–2095.
134 F. Matsumoto, S. M. Vorpahl, J. Q. Banks, E. Sengupta and D. S. Ginger, *J. Phys. Chem. C*, 2015, **119**, 20810–20816.
135 Y. Dkhissi, H. Weerasinghe, S. Meyer, I. Benesperi, U. Bach, L. Spiccia, R. A. Caruso and Y.-B. Cheng, *Nano Energy*, 2016, **22**, 211–222.
136 J. Idigoras, A. Todinova, J. R. Sanchez-Valencia, A. Barranco, A. Borras and J. A. Anta, *Phys. Chem. Chem. Phys.*, 2016, **18**, 13583–13590.
137 Y. Dkhissi, S. Meyer, D. Chen, H. C. Weerasinghe, L. Spiccia, Y. B. Cheng and R. A. Caruso, *ChemSusChem*, 2016, **9**, 687–695.
138 M. Jørgensen, K. Norrman and F. C. Krebs, *Sol. Energy Mater. Sol. Cells*, 2008, **92**, 686–714.
139 S. Kumar and A. Dhar, *ACS Appl. Mater. Interfaces*, 2016, **8**, 18309–18320.
140 L. Zheng, Y. H. Chung, Y. Ma, L. Zhang, L. Xiao, Z. Chen, S. Wang, B. Qu and Q. Gong, *Chem. Commun.*, 2014, **50**, 11196–11199.
141 J. You, L. Meng, T. B. Song, T. F. Guo, Y. M. Yang, W. H. Chang, Z. Hong, H. Chen, H. Zhou, Q. Chen, Y. Liu, N. De Marco and Y. Yang, *Nat. Nanotechnol.*, 2015, **11**, 75–81.
142 Q. Bao, X. Liu, S. Braun and M. Fahlman, *Adv. Energy Mater.*, 2014, **4**, 1301272.
143 L. Zhao, R. A. Kerner, Z. Xiao, Y. L. Lin, K. M. Lee, J. Schwartz and B. P. Rand, *ACS Energy Lett.*, 2016, **1**, 595–602.
144 K. E. A. Hooper, H. K. H. Lee, M. J. Newman, S. Meroni, J. Baker, T. M. Watson and W. C. Tsoi, *Phys. Chem. Chem. Phys.*, 2017, **19**, 5246–5253.
145 P. Darvishzadeh, M. Babanezhad, R. Ahmadi and N. E. Gorji, *Mater. Des.*, 2017, **114**, 339–344.
146 H. Sohrabpoor, G. Puccetti and N. E. Gorji, *RSC Adv.*, 2016, **6**, 49328–49334.
147 P. Bhatt, M. Kumar, P. Chandra Kant, M. K. Pandey and B. Tripathi, *Org. Electron.*, 2016, **39**, 258–266.
148 H. J. Snaith, A. Abate, J. M. Ball, G. E. Eperon, T. Leijtens, N. K. Noel, S. D. Stranks, J. T.-W. Wang, K. Wojciechowski and W. Zhang, *J. Phys. Chem. Lett.*, 2014, **5**, 1511–1515.
149 T. M. Brenner, D. A. Egger, L. Kronik, G. Hodes and D. Cahen, *Nat. Rev. Mater.*, 2016, **1**, 15007.
150 L. Cheng, G. Antonio, Z. Yu and H. Sven, *J. Phys.: Condens. Matter*, 2017, **29**, 193001.
151 R. T. Ginting, M.-K. Jeon, K.-J. Lee, W.-Y. Jin, T.-W. Kim and J.-W. Kang, *J. Mater. Chem. A*, 2017, **5**, 4527–4534.
152 S. Cacovich, G. Divitini, C. Ireland, F. Matteocci, A. Di Carlo and C. Ducati, *ChemSusChem*, 2016, **9**, 2673–2678.
153 Y. Yuan and J. Huang, *Acc. Chem. Res.*, 2016, **49**, 286–293.
154 G. H. Vineyard, *J. Phys. Chem. Solids*, 1957, **3**, 121–127.
155 L. Tomas, E. T. Hoke, G. Giulia, D. J. Slotcavage, G. E. Eperon, J. M. Ball, D. B. Michele, A. R. Bowring, M. Nicola and W. Konrad, *Adv. Energy Mater.*, 2015, **5**, 1500962.
156 Y. Shao, Z. Xiao, C. Bi, Y. Yuan and J. Huang, *Nat. Commun.*, 2014, **5**, 5784.
157 J.-W. Lee, S.-G. Kim, S.-H. Bae, D.-K. Lee, O. Lin, Y. Yang and N.-G. Park, *Nano Lett.*, 2017, **17**, 4270–4276.
158 J. S. Yun, J. Seidel, J. Kim, A. M. Soufiani, S. Huang, J. Lau, N. J. Jeon, S. I. Seok, M. A. Green and A. Ho-Baillie, *Adv. Energy Mater.*, 2016, **6**, 1600330.
159 A. Buin, P. Pietsch, J. Xu, O. Voznyy, A. H. Ip, R. Comin and E. H. Sargent, *Nano Lett.*, 2014, **14**, 6281–6286.
160 T. A. Berhe, W.-N. Su, C.-H. Chen, C.-J. Pan, J.-H. Cheng, H.-M. Chen, M.-C. Tsai, L.-Y. Chen, A. A. Dubale and B.-J. Hwang, *Energy Environ. Sci.*, 2016, **9**, 323–356.
161 W. Zhu, C. Bao, F. Li, T. Yu, H. Gao, Y. Yi, J. Yang, G. Fu, X. Zhou and Z. Zou, *Nano Energy*, 2016, **19**, 17–26.
162 Y. Chen, T. Chen and L. Dai, *Adv. Mater.*, 2015, **27**, 1053–1059.
163 Q. Jiang, D. Rebollar, J. Gong, E. L. Piacentino, C. Zheng and T. Xu, *Angew. Chem.*, 2015, **54**, 7617–7620.
164 Q. Tai, P. You, H. Sang, Z. Liu, C. Hu, H. L. W. Chan and F. Yan, *Nat. Commun.*, 2016, **7**, 11105.
165 Y.-H. Chiang, M.-H. Li, H.-M. Cheng, P.-S. Shen and P. Chen, *ACS Appl. Mater. Interfaces*, 2017, **9**, 2403–2409.
166 S. Yang, W. Liu, L. Zuo, X. Zhang, T. Ye, J. Chen, C.-Z. Li, G. Wu and H. Chen, *J. Mater. Chem. A*, 2016, **4**, 9430–9436.
167 S. Nagane, U. Bansode, O. Game, S. Chhatre and S. Ogale, *Chem. Commun.*, 2014, **50**, 9741–9744.
168 J. Chen, Y. Rong, A. Mei, Y. Xiong, T. Liu, Y. Sheng, P. Jiang, L. Hong, Y. Guan, X. Zhu, X. Hou, M. Duan, J. Zhao, X. Li and H. Han, *Adv. Energy Mater.*, 2016, **6**, 1502009.
169 J.-W. Lee, D.-H. Kim, H.-S. Kim, S.-W. Seo, S. M. Cho and N.-G. Park, *Adv. Energy Mater.*, 2015, **5**, 1501310.
170 Z. Li, M. Yang, J.-S. Park, S.-H. Wei, J. J. Berry and K. Zhu, *Chem. Mater.*, 2016, **28**, 284–292.
171 Y. Chang, L. Wang, J. Zhang, Z. Zhou, C. Li, B. Chen, L. Etgar, G. Cui and S. Pang, *J. Mater. Chem. A*, 2017, **5**, 4803–4808.
172 C. Yi, J. Luo, S. Meloni, A. Boziki, N. Ashari-Astani, C. Gratzel, S. M. Zakeeruddin, U. Rothlisberger and M. Gratzel, *Energy Environ. Sci.*, 2016, **9**, 656–662.
173 I. C. Smith, E. T. Hoke, D. Solis-Ibarra, M. D. McGehee and H. I. Karunadasa, *Angew. Chem.*, 2014, **53**, 11232–11235.
174 L. N. Quan, M. Yuan, R. Comin, O. Voznyy, E. M. Beauregard, S. Hoogland, A. Buin, A. R. Kirmani, K. Zhao, A. Amassian, D. H. Kim and E. H. Sargent, *J. Am. Chem. Soc.*, 2016, **138**, 2649–2655.

175 N. Li, Z. Zhu, C.-C. Chueh, H. Liu, B. Peng, A. Petrone, X. Li, L. Wang and A. K. Y. Jen, *Adv. Energy Mater.*, 2017, **7**, 1601307.
176 D. H. Cao, C. C. Stoumpos, O. K. Farha, J. T. Hupp and M. G. Kanatzidis, *J. Am. Chem. Soc.*, 2015, **137**, 7843–7850.
177 J.-F. Liao, H.-S. Rao, B.-X. Chen, D.-B. Kuang and C.-Y. Su, *J. Mater. Chem. A*, 2017, **5**, 2066–2072.
178 W. Jiang, J. Ying, W. Zhou, K. Shen, X. Liu, X. Gao, F. Guo, Y. Gao and T. Yang, *Chem. Phys. Lett.*, 2016, **658**, 71–75.
179 K. Yao, X. Wang, Y.-X. Xu, F. Li and L. Zhou, *Chem. Mater.*, 2016, **28**, 3131–3138.
180 K. Yao, X. Wang, F. Li and L. Zhou, *Chem. Commun.*, 2015, **51**, 15430–15433.
181 S. Sourisseau, N. Louvain, W. Bi, N. Mercier, D. Rondeau, J.-Y. Buzaré and C. Legein, *Inorg. Chem.*, 2007, **46**, 6148–6154.
182 X. Hong, T. Ishihara and A. V. Nurmikko, *Phys. Rev. B: Condens. Matter Mater. Phys.*, 1992, **45**, 6961–6964.
183 H. Tsai, W. Nie, J.-C. Blancon, C. C. Stoumpos, R. Asadpour, B. Harutyunyan, A. J. Neukirch, R. Verduzco, J. J. Crochet, S. Tretiak, L. Pedesseau, J. Even, M. A. Alam, G. Gupta, J. Lou, P. M. Ajayan, M. J. Bedzyk, M. G. Kanatzidis and A. D. Mohite, *Nature*, 2016, **536**, 312–316.
184 J. Cao, F. Wang, H. Yu, Y. Zhou, H. Lu, N. Zhao and C.-P. Wong, *J. Mater. Chem. A*, 2016, **4**, 10223–10230.
185 H.-S. Ko, J.-W. Lee and N.-G. Park, *J. Mater. Chem. A*, 2015, **3**, 8808–8815.
186 S. Yuan, Z. Qiu, C. Gao, H. Zhang, Y. Jiang, C. Li, J. Yu and B. Cao, *ACS Appl. Mater. Interfaces*, 2016, **8**, 22238–22245.
187 G. Li, T. Zhang and Y. Zhao, *J. Mater. Chem. A*, 2015, **3**, 19674–19678.
188 L. Yang, J. Wang and W. W. Leung, *ACS Appl. Mater. Interfaces*, 2015, **7**, 14614–14619.
189 K. M. Boopathi, R. Mohan, T.-Y. Huang, W. Budiawan, M.-Y. Lin, C.-H. Lee, K.-C. Ho and C.-W. Chu, *J. Mater. Chem. A*, 2016, **4**, 1591–1597.
190 H.-J. Yen, P.-W. Liang, C.-C. Chueh, Z. Yang, A. K. Y. Jen and H.-L. Wang, *ACS Appl. Mater. Interfaces*, 2016, **8**, 14513–14520.
191 X. Li, M. I. Dar, C. Yi, J. Luo, M. Tschumi, S. M. Zakeeruddin, M. K. Nazeeruddin, H. Han and M. Gratzel, *Nat. Chem.*, 2015, **7**, 703–711.
192 B. Xia, Z. Wu, H. Dong, J. Xi, W. Wu, T. Lei, K. Xi, F. Yuan, B. Jiao, L. Xiao, Q. Gong and X. Hou, *J. Mater. Chem. A*, 2016, **4**, 6295–6303.
193 S. Casaluci, L. Cinà, A. Pockett, P. S. Kubiak, R. G. Niemann, A. Reale, A. Di Carlo and P. J. Cameron, *J. Power Sources*, 2015, **297**, 504–510.
194 X. Sun, C. Zhang, J. Chang, H. Yang, H. Xi, G. Lu, D. Chen, Z. Lin, X. Lu, J. Zhang and Y. Hao, *Nano Energy*, 2016, **28**, 417–425.
195 S. Wang, L. Wang, L. Zhang, L. Chang, L. Wang and J. Wang, *Sol. Energy Mater. Sol. Cells*, 2017, **163**, 120–124.
196 B. Wang and T. Chen, *Adv. Sci.*, 2015, **3**, 1500262.
197 A. Mei, X. Li, L. Liu, Z. Ku, T. Liu, Y. Rong, M. Xu, M. Hu, J. Chen, Y. Yang, M. Grätzel and H. Han, *Science*, 2014, **345**, 295–298.
198 E. W. Jones, P. J. Holliman, A. Connell, M. L. Davies, J. Baker, R. J. Hobbs, S. Ghosh, L. Furnell, R. Anthony and C. Pleydell-Pearce, *Chem. Commun.*, 2016, **52**, 4301–4304.
199 J. S. Manser, M. I. Saidaminov, J. A. Christians, O. M. Bakr and P. V. Kamat, *Acc. Chem. Res.*, 2016, **49**, 330–338.
200 D. Shi, V. Adinolfi, R. Comin, M. Yuan, E. Alarousu, A. Buin, Y. Chen, S. Hoogland, A. Rothenberger, K. Katsiev, Y. Losovyj, X. Zhang, P. A. Dowben, O. F. Mohammed, E. H. Sargent and O. M. Bakr, *Science*, 2015, **347**, 519–522.
201 Q. Dong, Y. Fang, Y. Shao, P. Mulligan, J. Qiu, L. Cao and J. Huang, *Science*, 2015, **347**, 967–970.
202 W. Peng, L. Wang, B. Murali, K. T. Ho, A. Bera, N. Cho, C. F. Kang, V. M. Burlakov, J. Pan and L. Sinatra, *Adv. Mater.*, 2016, **28**, 3383–3390.
203 B. Wu, N. Huy Tiep, Z. Ku, G. Han, D. Giovanni, N. Mathews, H. J. Fan and T. C. Sum, *Adv. Energy Mater.*, 2016, **6**, 1600551.
204 S. Y. Leblebici, L. Leppert, Y. Li, S. E. Reyes-Lillo, S. Wickenburg, E. Wong, J. Lee, M. Melli, D. Ziegler, D. K. Angell, D. F. Ogletree, P. D. Ashby, F. M. Toma, J. B. Neaton, I. D. Sharp and A. Weber-Bargioni, *Nat. Energy*, 2016, **1**, 16093.
205 S. Feng, Y. Yang, M. Li, J. Wang, Z. Cheng, J. Li, G. Ji, G. Yin, F. Song and Z. Wang, *ACS Appl. Mater. Interfaces*, 2016, **8**, 14503–14512.
206 D. Song, D. Wei, P. Cui, M. Li, Z. Duan, T. Wang, J. Ji, Y. Li, J. M. Mbengue, Y. Li, Y. He, M. Trevor and N.-G. Park, *J. Mater. Chem. A*, 2016, **4**, 6091–6097.
207 S. Ito, G. Mizuta, S. Kanaya, H. Kanda, T. Nishina, S. Nakashima, H. Fujisawa, M. Shimizu, Y. Haruyama and H. Nishino, *Phys. Chem. Chem. Phys.*, 2016, **18**, 27102–27108.
208 J. Yin, J. Cao, X. He, S. Yuan, S. Sun, J. Li, N. Zheng and L. Lin, *J. Mater. Chem. A*, 2015, **3**, 16860–16866.
209 H. Choi, C.-K. Mai, H.-B. Kim, J. Jeong, S. Song, G. C. Bazan, J. Y. Kim and A. J. Heeger, *Nat. Commun.*, 2015, **6**, 7348.
210 Q. Wang, C.-C. Chueh, M. Eslamian and A. K. Y. Jen, *ACS Appl. Mater. Interfaces*, 2016, **8**, 32068–32076.
211 P. Wang, J. Zhao, J. Liu, L. Wei, Z. Liu, L. Guan and G. Cao, *J. Power Sources*, 2017, **339**, 51–60.
212 G. Yang, C. Wang, H. Lei, X. Zheng, P. Qin, L. Xiong, X. Zhao, Y. Yan and G. Fang, *J. Mater. Chem. A*, 2017, **5**, 1658–1666.
213 H. Si, Q. Liao, Z. Zhang, Y. Li, X. Yang, G. Zhang, Z. Kang and Y. Zhang, *Nano Energy*, 2016, **22**, 223–231.
214 W.-Y. Chen, L.-L. Deng, S.-M. Dai, X. Wang, C.-B. Tian, X.-X. Zhan, S.-Y. Xie, R.-B. Huang and L.-S. Zheng, *J. Mater. Chem. A*, 2015, **3**, 19353–19359.
215 H. Rao, W. Sun, S. Ye, W. Yan, Y. Li, H. Peng, Z. Liu, Z. Bian and C. Huang, *ACS Appl. Mater. Interfaces*, 2016, **8**, 7800–7805.
216 W. Sun, Y. Li, S. Ye, H. Rao, W. Yan, H. Peng, Y. Li, Z. Liu, S. Wang, Z. Chen, L. Xiao, Z. Bian and C. Huang, *Nanoscale*, 2016, **8**, 10806–10813.
217 Y. Li, S. Ye, W. Sun, W. Yan, Y. Li, Z. Bian, Z. Liu, S. Wang and C. Huang, *J. Mater. Chem. A*, 2015, **3**, 18389–18394.

218 Q. Liu, M.-C. Qin, W.-J. Ke, X.-L. Zheng, Z. Chen, P.-L. Qin, L.-B. Xiong, H.-W. Lei, J.-W. Wan, J. Wen, G. Yang, J.-J. Ma, Z.-Y. Zhang and G.-J. Fang, *Adv. Funct. Mater.*, 2016, **26**, 6069–6075.
219 P. L. Qin, H. W. Lei, X. L. Zheng, Q. Liu, H. Tao, G. Yang, W. J. Ke, L. B. Xiong, M. C. Qin and X. Z. Zhao, *Adv. Mater. Interfaces*, 2016, **3**, 1500799.
220 A. Agresti, S. Pescetelli, L. Cinà, D. Konios, G. Kakavelakis, E. Kymakis and A. D. Carlo, *Adv. Funct. Mater.*, 2016, **26**, 2686–2694.
221 M. M. Tavakoli, R. Tavakoli, Z. Nourbakhsh, A. Waleed, U. S. Virk and Z. Fan, *Adv. Mater. Interfaces*, 2016, **3**, 1500790.
222 H. Chen, Y. Hou, C. E. Halbig, S. Chen, H. Zhang, N. Li, F. Guo, X. Tang, N. Gasparini, I. Levchuk, S. Kahmann, C. O. Ramirez Quiroz, A. Osvet, S. Eigler and C. J. Brabec, *J. Mater. Chem. A*, 2016, **4**, 11604–11610.
223 Y. Ogomi, A. Morita, S. Tsukamoto, T. Saitho, Q. Shen, T. Toyoda, K. Yoshino, S. S. Pandey, T. Ma and S. Hayase, *J. Phys. Chem. C*, 2014, **118**, 16651–16659.
224 D. Bi, P. Gao, R. Scopelliti, E. Oveisi, J. Luo, M. Grätzel, A. Hagfeldt and M. K. Nazeeruddin, *Adv. Mater.*, 2016, **28**, 2910–2915.
225 N. Tripathi, Y. Shirai, M. Yanagida, A. Karen and K. Miyano, *ACS Appl. Mater. Interfaces*, 2016, **8**, 4644–4650.
226 S. Yang, Y. Wang, P. Liu, Y.-B. Cheng, H. J. Zhao and H. G. Yang, *Nat. Energy*, 2016, **1**, 15016.
227 H. Xiong, Y. Rui, Y. Li, Q. Zhang and H. Wang, *J. Mater. Chem. C*, 2016, **4**, 6848–6854.
228 B. Li, C. Fei, K. Zheng, X. Qu, T. Pullerits, G. Cao and J. Tian, *J. Mater. Chem. A*, 2016, **4**, 17018–17024.
229 S. Masi, S. Colella, A. Listorti, V. Roiati, A. Liscio, V. Palermo, A. Rizzo and G. Gigli, *Sci. Rep.*, 2015, **5**, 7725.
230 C. Ran, Y. Chen, W. Gao, M. Wang and L. Dai, *J. Mater. Chem. A*, 2016, **4**, 8566–8572.
231 Y. Zhao, J. Wei, H. Li, Y. Yan, W. Zhou, D. Yu and Q. Zhao, *Nat. Commun.*, 2016, **7**, 10228.
232 N. Rajamanickam, S. Kumari, V. K. Vendra, B. W. Lavery, J. Spurgeon, T. Druffel and M. K. Sunkara, *Nanotechnology*, 2016, **27**, 235404.
233 J. Wei, H. Li, Y. Zhao, W. Zhou, R. Fu, Y. Leprince-Wang, D. Yu and Q. Zhao, *Nano Energy*, 2016, **26**, 139–147.
234 Y. Guo, K. Shoyama, W. Sato and E. Nakamura, *Adv. Energy Mater.*, 2016, **6**, 1502317.
235 H. Wang, Y. Rahaq and V. Kumar, *Sci. Rep.*, 2016, **6**, 29567.
236 L. K. Ono, S. R. Raga, M. Remeika, A. J. Winchester, A. Gabe and Y. Qi, *J. Mater. Chem. A*, 2015, **3**, 15451–15456.
237 B. Xu, J. Huang, H. Ågren, L. Kloo, A. Hagfeldt and L. Sun, *ChemSusChem*, 2014, **7**, 3252–3256.
238 M. C. Jung, S. R. Raga, L. K. Ono and Y. Qi, *Sci. Rep.*, 2015, **5**, 9863.
239 L. Badia, E. Mas-Marzá, R. S. Sánchez, E. M. Barea, J. Bisquert and I. Mora-Seró, *APL Mater.*, 2014, **2**, 717–731.
240 M. Li, Z.-K. Wang, Y.-G. Yang, Y. Hu, S.-L. Feng, J.-M. Wang, X.-Y. Gao and L.-S. Liao, *Adv. Energy Mater.*, 2016, **6**, 1601156.
241 Y. Yue, N. Salim, Y. Wu, X. Yang, A. Islam, W. Chen, J. Liu, E. Bi, F. Xie, M. Cai and L. Han, *Adv. Mater.*, 2016, **28**, 10738–10743.
242 J. Xu, O. Voznyy, R. Comin, X. Gong, G. Walters, M. Liu, P. Kanjanaboos, X. Lan and E. H. Sargent, *Adv. Mater.*, 2016, **28**, 2807–2815.
243 F. Wang, M. Endo, S. Mouri, Y. Miyauchi, Y. Ohno, A. Wakamiya, Y. Murata and K. Matsuda, *Nanoscale*, 2016, **8**, 11882–11888.
244 H. Zhang, H. Wang, W. Chen and A. K. Y. Jen, *Adv. Mater.*, 2016, **29**, 1604984.
245 B. Koo, H. Jung, M. Park, J. Y. Kim, H. J. Son, J. Cho and M. J. Ko, *Adv. Funct. Mater.*, 2016, **26**, 5400–5407.
246 S. N. Habisreutinger, B. Wenger, H. J. Snaith and R. J. Nicholas, *ACS Energy Lett.*, 2017, **2**, 622–628.
247 J. Cao, Y. M. Liu, X. Jing, J. Yin, J. Li, B. Xu, Y. Z. Tan and N. Zheng, *J. Am. Chem. Soc.*, 2015, **137**, 10914–10917.
248 H.-C. Liao, T. L. D. Tam, P. Guo, Y. Wu, E. F. Manley, W. Huang, N. Zhou, C. M. M. Soe, B. Wang, M. R. Wasielewski, L. X. Chen, M. G. Kanatzidis, A. Facchetti, R. P. H. Chang and T. J. Marks, *Adv. Energy Mater.*, 2016, **6**, 1600502.
249 G. Kakavelakis, T. Maksudov, D. Konios, I. Paradisanos, G. Kioseoglou, E. Stratakis and E. Kymakis, *Adv. Energy Mater.*, 2016, **7**, 1602120.
250 Y. Bai, Q. Dong, Y. Shao, Y. Deng, Q. Wang, L. Shen, D. Wang, W. Wei and J. Huang, *Nat. Commun.*, 2016, **7**, 12806.
251 Z. Zhu, Y. Bai, X. Liu, C. C. Chueh, S. Yang and A. K. Y. Jen, *Adv. Mater.*, 2016, **28**, 6478–6484.
252 W. Chen, Y. Wu, Y. Yue, J. Liu, W. Zhang, X. Yang, H. Chen, E. Bi, I. Ashraful and M. Grätzel, *Science*, 2015, **350**, 944–948.
253 Z. Wang, D. P. McMeekin, N. Sakai, S. van Reenen, K. Wojciechowski, J. B. Patel, M. B. Johnston and H. J. Snaith, *Adv. Mater.*, 2017, **29**, 1604186.
254 S. Shao, Z. Chen, H. H. Fang, G. H. ten Brink, D. Bartesaghi, S. Adjokatse, L. J. A. Koster, B. J. Kooi, A. Facchetti and M. A. Loi, *J. Mater. Chem. A*, 2016, **4**, 2419–2426.
255 K. O. Brinkmann, J. Zhao, N. Pourdavoud, T. Becker, T. Hu, S. Olthof, K. Meerholz, L. Hoffmann, T. Gahlmann, R. Heiderhoff, M. F. Oszajca, N. A. Luechinger, D. Rogalla, Y. Chen, B. Cheng and T. Riedl, *Nat. Commun.*, 2017, **8**, 13938.
256 C.-Y. Chang, W.-K. Huang, Y.-C. Chang, K.-T. Lee and C.-T. Chen, *J. Mater. Chem. A*, 2016, **4**, 640–648.
257 Z. Zhu, C. C. Chueh, F. Lin and A. K. Y. Jen, *Adv. Sci.*, 2016, **3**, 1600027.
258 M. Kaltenbrunner, G. Adam, E. D. Glowacki, M. Drack, R. Schwodiauer, L. Leonat, D. H. Apaydin, H. Groiss, M. C. Scharber, M. S. White, N. S. Sariciftci and S. Bauer, *Nat. Mater.*, 2015, **14**, 1032–1039.
259 F. Wang, A. Shimazaki, F. Yang, K. Kanahashi, K. Matsuki, Y. Miyauchi, T. Takenobu, A. Wakamiya, Y. Murata and K. Matsuda, *J. Phys. Chem. C*, 2017, **121**, 1562–1568.
260 J. Zhang, Z. Hu, L. Huang, G. Yue, J. Liu, X. Lu, Z. Hu, M. Shang, L. Han and Y. Zhu, *Chem. Commun.*, 2015, **51**, 7047–7050.
261 Q. Wang, Q. Dong, T. Li, A. Gruverman and J. Huang, *Adv. Mater.*, 2016, **28**, 6734–6739.

262 D. Koushik, W. J. H. Verhees, Y. Kuang, S. Veenstra, D. Zhang, M. A. Verheijen, M. Creatore and R. E. I. Schropp, *Energy Environ. Sci.*, 2017, **10**, 91–100.
263 Y. Kato, L. K. Ono, M. V. Lee, S. Wang, S. R. Raga and Y. Qi, *Adv. Mater. Interfaces*, 2015, **2**, 1500195.
264 K. Domanski, J.-P. Correa-Baena, N. Mine, M. K. Nazeeruddin, A. Abate, M. Saliba, W. Tress, A. Hagfeldt and M. Grätzel, *ACS Nano*, 2016, **10**, 6306–6314.
265 Y. Deng, Q. Dong, C. Bi, Y. Yuan and J. Huang, *Adv. Energy Mater.*, 2016, **6**, 1600372.
266 J. Zhao, X. Zheng, Y. Deng, T. Li, Y. Shao, A. Gruverman, J. Shield and J. Huang, *Energy Environ. Sci.*, 2016, **9**, 3650–3656.
267 M. Acik and S. B. Darling, *J. Mater. Chem. A*, 2016, **4**, 6185–6235.
268 K. Cao, Z. Zuo, J. Cui, Y. Shen, T. Moehl, S. M. Zakeeruddin, M. Grätzel and M. Wang, *Nano Energy*, 2015, **17**, 171–179.
269 I. Hwang, I. Jeong, J. Lee, M. J. Ko and K. Yong, *ACS Appl. Mater. Interfaces*, 2015, **7**, 17330–17336.
270 X. Li, M. Tschumi, H. Han, S. S. Babkair, R. A. Alzubaydi, A. A. Ansari, S. S. Habib, M. K. Nazeeruddin, S. M. Zakeeruddin and D. M. Grätzel, *Energy Technol.*, 2015, **3**, 551–555.
271 Q. Dong, F. Liu, M. K. Wong, H. W. Tam, A. B. Djurišić, A. Ng, C. Surya, W. K. Chan and A. M. C. Ng, *ChemSusChem*, 2016, **9**, 2597–2603.
272 H. C. Weerasinghe, Y. Dkhissi, A. D. Scully, R. A. Caruso and Y.-B. Cheng, *Nano Energy*, 2015, **18**, 118–125.
273 F. Matteocci, L. Cinà, E. Lamanna, S. Cacovich, G. Divitini, P. A. Midgley, C. Ducati and A. Di Carlo, *Nano Energy*, 2016, **30**, 162–172.
274 Y. Han, S. Meyer, Y. Dkhissi, K. Weber, J. M. Pringle, U. Bach, L. Spiccia and Y.-B. Cheng, *J. Mater. Chem. A*, 2015, **3**, 8139–8147.
275 T. J. Wilderspin, F. De Rossi and T. M. Watson, *Sol. Energy*, 2016, **139**, 426–432.
276 X. Guo, C. McCleese, W.-C. Lin and C. Burda, *RSC Adv.*, 2016, **6**, 60620–60625.
277 S.-W. Lee, S. Kim, S. Bae, K. Cho, T. Chung, L. E. Mundt, S. Lee, S. Park, H. Park, M. C. Schubert, S. W. Glunz, Y. Ko, Y. Jun, Y. Kang, H.-S. Lee and D. Kim, *Sci. Rep.*, 2016, **6**, 38150.
278 F. Lang, N. H. Nickel, J. Bundesmann, S. Seidel, A. Denker, S. Albrecht, V. V. Brus, J. Rappich, B. Rech, G. Landi and H. C. Neitzert, *Adv. Mater.*, 2016, **28**, 8726–8731.
279 W. Nie, J.-C. Blancon, A. J. Neukirch, K. Appavoo, H. Tsai, M. Chhowalla, M. A. Alam, M. Y. Sfeir, C. Katan, J. Even, S. Tretiak, J. J. Crochet, G. Gupta and A. D. Mohite, *Nat. Commun.*, 2016, **7**, 11574.
280 X. Zhao, H.-S. Kim, J.-Y. Seo and N.-G. Park, *ACS Appl. Mater. Interfaces*, 2017, **9**, 7148–7153.
281 R. S. Sanchez and E. Mas-Marza, *Sol. Energy Mater. Sol. Cells*, 2016, **158**, 189–194.
282 A. K. Jena, M. Ikegami and T. Miyasaka, *ACS Energy Lett.*, 2017, **2**, 1760–1761.
283 W. H. Nguyen, C. D. Bailie, E. L. Unger and M. D. McGehee, *J. Am. Chem. Soc.*, 2014, **136**, 10996–11001.